# 5  More on importance sampling Monte Carlo methods for lattice systems

## 5.1 CLUSTER FLIPPING METHODS

### 5.1.1 Fortuin–Kasteleyn theorem

Advances in simulational methods sometimes have their origin in unusual places; such is the case with an entire class of methods which attempt to beat critical slowing down in spin models on lattices by flipping correlated clusters of spins in an intelligent way instead of simply attempting single spin-flips. The first steps were taken by Fortuin and Kasteleyn (Kasteleyn and Fortuin, 1969; Fortuin and Kasteleyn, 1972), who showed that it was possible to map a ferromagnetic Potts model onto a corresponding percolation model. The reason that this observation is so important is that in the percolation problem states are produced by throwing down particles, or bonds, in an uncorrelated fashion; hence there is *no critical slowing down*. In contrast, as we have already mentioned, the $q$-state Potts model when treated using standard Monte Carlo methods suffers from slowing down. (Even for large $q$ where the transition is first order, the time scales can become quite long.) The Fortuin–Kasteleyn transformation thus allows us to map a problem with slow critical relaxation into one where such effects are largely absent. (As we shall see, not all slowing down is eliminated, but the problem is reduced quite dramatically.)

The partition function of the $q$-state Potts model (see Eqn. (2.43)) is

$$Z = \sum_{\{\sigma_i\}} e^{2K\sum_{i,j}(\delta_{\sigma_i\sigma_j}-1)}, \tag{5.1}$$

where $K = \mathcal{J}/k_{\mathrm{B}}T$ and the sum over $\{\sigma_i\}$ is over all states of the system. The transformation replaces each pair of interacting Potts spins on the lattice by a bond on an equivalent lattice with probability

$$p = 1 - e^{-2K\delta_{\sigma_i\sigma_j}}. \tag{5.2}$$

This means, of course, that there is only a non-zero probability of bonds being drawn if the pair of spins on the original lattice is in the same state. This process must be carried out for all pairs of spins, leaving behind a lattice with bonds which connect some sites and forming a set of clusters with different sizes and shapes. Note that all spins in each cluster must have the same value. The spins may then be integrated out (leaving a factor of $q$ behind for each
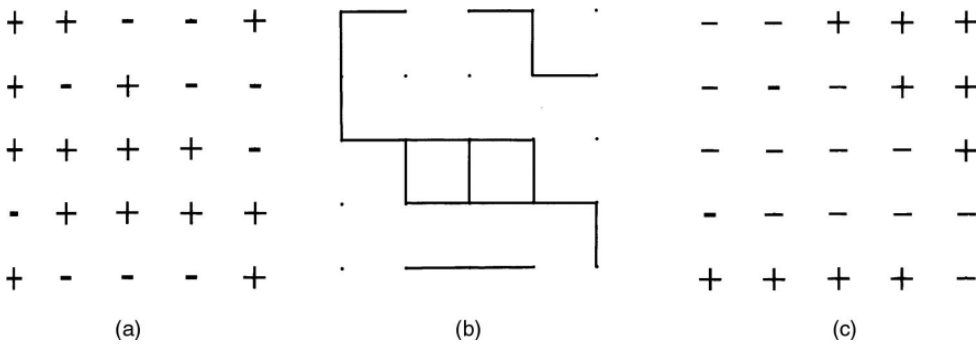
144

Fig. 5.1 Schematic view of the Swendsen–Wang algorithm for an Ising model: (a) original spin configuration; (b) clusters formed; (c) 'decorated' clusters.

cluster) and for the $N_c$ clusters which remain (including single site clusters) the resultant partition function is

$$Z = \sum_{\text{bonds}} p^b (1-p)^{(N_b - b)} q^{N_c}, \qquad (5.3)$$

where $b$ is the number of bonds and $N_b$ is the total number of possible bonds. The quantity $(1-p)$ is simply the probability that no bond exists between a pair of sites. Thus, the Potts and percolation problems are equivalent. This equivalence was first exploited by Sweeny (1983) who generated graph configurations directly for the weighted percolation problem and showed that this was a more efficient approach than using the Metropolis method. In the following two sub-sections we shall demonstrate two particularly simple, different ways in which this equivalence may be exploited to devise new Monte Carlo methods which work 'directly' with the spin systems.

### 5.1.2 Swendsen–Wang method

The first use of the Fortuin–Kasteleyn transformation in Monte Carlo simulations was by Swendsen and Wang (1987); and although this is seldom the most efficient method, it remains an important tool. Just as in the Metropolis method, we may begin with any sort of an initial spin configuration. We then proceed through the lattice, placing bonds between each pair of spins with the probability given by Eqn. (5.2). A Hoshen–Kopelman method (see Section 3.6) is used to identify all clusters of sites which are produced by a connected network of bonds. Each cluster is then randomly assigned a new spin value, using a random number, i.e. each site in a cluster must have the same new spin value. The bonds are 'erased' and a new spin configuration is produced. See Fig. 5.1 for a schematic representation of the implementation of this algorithm. Since the probability of placing a bond between pairs of sites depends on temperature, it is clear that the resultant cluster distributions will vary dramatically with temperature. At very high temperature the clusters will tend to be quite small. At very low temperature virtually all sites with

nearest neighbors in the same state will wind up in the same cluster and there will be a tendency for the system to oscillate back and forth between quite similar structures. Near a critical point, however, a quite rich array of clusters is produced and the net result is that each configuration differs substantially from its predecessor; hence, critical slowing down is reduced. In addition to the above intuitive argument, the reduction in characteristic time scales has been measured directly. It is thus known that the dynamic critical exponent $z$ is reduced from a value of just over 2 for Metropolis single-site spin–flipping to a value of about 0 (i.e. log) in two dimensions and $\sim 0.5$ in three dimensions (Wang, 1990). Please don't forget, however, that the overall performance of the algorithm also depends strongly on the complexity of the code which is usually much greater than for single spin-flip methods. Hence, for small lattices the Swendsen–Wang technique may not offer much advantage (or may actually be slower in real time), but for sufficiently large lattices it will eventually become more efficient.

---

**Swendsen–Wang algorithm for a $q$-state Potts model**

(1)  Choose a spin.
(2)  Calculate $p = 1 - e^{-2K\delta_{\sigma_i \sigma_j}}$ for each nearest neighbor.
(3)  If $p < 1$, generate a random number $0 < rng < 1$; if $rng < p$ place a bond between sites $i$ and $j$.
(4)  Choose the next spin and go to (2) until all bonds have been considered.
(5)  Apply the Hoshen–Kopelman algorithm to identify all clusters.
(6)  Choose a cluster.
(7)  Generate a random integer $1 \leq R_i \leq q$.
(8)  Assign $\sigma_i = R_i$ to all spins in the cluster.
(9)  Choose another cluster and go to (7).
(10)  When all clusters have been considered, go to (1).

---

This method may be extended to more complicated systems if one gives a little thought to modification. Magnetic fields can be included using two equivalent methods: either a 'ghost spin' is added which interacts with every spin in the system with a coupling equal to the magnetic field, or each cluster is treated as a single spin in a magnetic field whose strength is equal to the product of the field times the size of the cluster. If the interactions in an Ising model are antiferromagnetic instead of ferromagnetic, one simply places 'anti-bonds' between antiparallel spins with probability

$$p = 1 - e^{-2|K|} \tag{5.4}$$

and proceeds as before. A further extension is to antiferromagnetic $q$-state Potts models for which the groundstate is multiply degenerate (see Wang, 1989). Two different spin values are randomly chosen and all spins which have different values are frozen. The spins which are still free are then simulated

Fig. 5.2
Magnetization (–) and
percolation probability
(- -) plotted vs.
reduced temperature
for $L \times L$ Ising
models studied using
the Swendsen–Wang
algorithm. After De
Meo *et al.* (1990).
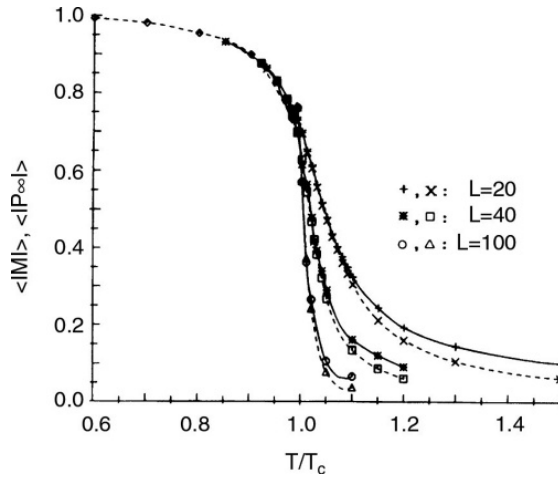


with the Swendsen–Wang algorithm with the frozen spins playing the role of quenched, non-interacting impurities. Two new spin values are chosen and the process is repeated. This method can also be applied to spin glass models but does not bring an improvement in performance due to the strong frustration.

The connection between cluster configurations and spin configuration raises a number of interesting issues which have been studied in detail by De Meo *et al.* (1990) for the Ising ferromagnet. In spite of the initial belief that the 'geometric clusters' formed by simply connecting *all* like spins in a given configuration could describe the Ising transition, it is clear that the actual 'physical clusters' which can be used for theoretical descriptions in terms of cluster theories are different. The Swendsen–Wang algorithm quite naturally selects only portions of a geometric cluster in creating new configurations. It is possible, however, to describe the thermal properties of a system in terms of the cluster properties, so one question becomes: just how well do the two agree? For the order parameter $M$ the estimate in terms of clusters is given by the sum over all clusters of like spin direction. In contrast, the percolation probability $P_\infty$ is determined only by the largest cluster. In a finite system the two may thus be expected to be different and indeed, as Fig. 5.2 shows, the finite size behaviors of the order parameter $M$ and the percolation probability $P_\infty$ are not the same. They also showed that for large lattices and $p < p_c$ in $d$-dimensions

$$\langle M \rangle \propto L^{-d/2}, \qquad L \to \infty, \tag{5.5a}$$

$$\langle P_\infty \rangle \propto L^{-d} \log L, \qquad L \to \infty. \tag{5.5b}$$

Related differences are present for the fluctuation quantities such as specific heat and susceptibility for which one has to separate out contributions from the clusters other than the largest one and those in the size of the largest cluster.

**Problem 5.1** Perform a Swendsen–Wang simulation of a 32 $\times$ 32 Ising square lattice with periodic boundary conditions at $T = 2.27 \ J/k_B$ and $T =$

$3.0\,J/k_B$. Determine the correlation times for the internal energy and compare the answers with the corresponding results for a Metropolis simulation at these temperatures. Comment on your findings.

### 5.1.3 Wolff method

One obvious shortcoming of the Swendsen–Wang approach is that significant effort is expended in dealing with small clusters as well as large ones. These small clusters do not contribute to the critical slowing down, so their consideration does not accelerate the algorithm. In order to partially eliminate this constraint, Wolff (1989a) proposed an alternative algorithm based on the Fortuin–Kasteleyn theorem in which single clusters are grown and flipped sequentially; the resultant performance generally exceeds that of the Swendsen–Wang method. The algorithm begins with the (random) choice of a single site. Bonds are then drawn to all nearest neighbors which are in the same state with probability

$$p = 1 - e^{-2K}. \tag{5.6}$$

One then moves to all sites in turn which have been connected to the initial site and places bonds between them and any of their nearest neighbors which are in the same state with probability given by Eqn. (5.6). The process continues until no new bonds are formed and the entire cluster of connected sites is then flipped. Another initial site is chosen and the process is then repeated. The Wolff dynamics has a smaller prefactor and smaller dynamic exponent than does the Swendsen–Wang method. Of course the measurement of Monte Carlo time is more complicated since a different number of spins is altered by each cluster flip. The generally accepted method of converting to MCS/site is to normalize the number of cluster flips by the mean fraction of sites $\langle c \rangle$ flipped at each step. The Monte Carlo time then becomes well-defined only after enough flips have occurred so that $\langle c \rangle$ is well defined. Later in this chapter we shall see just how important the Wolff algorithm can be for testing random number generators.

---

**Wolff cluster flipping method for the Ising model**

(1) Randomly choose a site.
(2) Draw bonds to all nearest neighbors with probability $p = 1 - e^{-2K\delta_{\sigma_i \sigma_j}}$.
(3) If bonds have been drawn to any nearest neighbor site $j$, draw bonds to all nearest neighbors $k$ of site $j$ with probability $p = 1 - e^{-2K\delta_{\sigma_j \sigma_k}}$.
(4) Repeat step (3) until no more new bonds are created.
(5) Flip all spins in the cluster.
(6) Go to (1).

---

**Problem 5.2** Perform a Wolff simulation of a 32 × 32 Ising square lattice with periodic boundary conditions at $T = 2.27$ $J/k_B$ and $T = 3.0$ $J/k_B$. Determine the correlation times for the internal energy and compare the answers with the corresponding results for a Metropolis simulation at these temperatures. Comment on your findings.

### 5.1.4 'Improved estimators'

In general, it may be possible to find multiple ways to calculate the same physical property of the system, and it may also turn out that the fluctuations in one estimator cancel more than for another estimator. (In earlier chapters we saw that the specific heat could be determined as a numerical derivative of the internal energy or from the fluctuations. The zero field susceptibility can be computed from the fluctuation of the order parameter or from the sum of the site–site correlation functions.) Since individual clusters are independent for the cluster flipping methods just discussed, for some quantities which can be calculated using cluster properties, 'noise reduction' occurs. It is then convenient to express various quantities in terms of clusters and use these expressions to answer the thermodynamic questions of interest (Sweeny, 1983; Wolff, 1988, 1990). Thus, for example, the susceptibility for $O(N)$ models is given by the mean cluster size, i.e.

$$\chi = \beta \langle |C| \rangle \tag{5.7}$$

where $|C|$ is the size of a cluster. The statistical error in the cluster definition of the susceptibility is smaller than that obtained using the fluctuations in the order parameter since the fluctuations due to the very small clusters cancel out. As discussed in the first section, however, for finite systems the behavior is not exactly the same as the true susceptibility, but in the thermodynamic limit it yields the same behavior. An improved estimator for the correlation function of the non-linear sigma model also yields substantial reduction in statistical error (Hasenbusch, 1995) and this property can be used for the classical spin systems that will be discussed shortly. The conclusion to which one might reasonably come is that not only the simulation method but also the method of analyzing the data needs careful consideration. We shall see in Chapter 7 just how important this consideration can be.

### 5.1.5 Invaded cluster algorithm

The cluster algorithms that have just been described represent a general approach to the simulational study of phase transitions with critical slowing down that is fundamentally different from the single spin-flip methods described in Chapter 4. The success of these cluster algorithms led to new variations that allow the method to 'sample' the critical region without a priori knowledge of $T_c$. (These methods should be generally effective so long as the bond percolation process has a percolation threshold that coincides with the phase transition.) One of these modified techniques, the invaded cluster
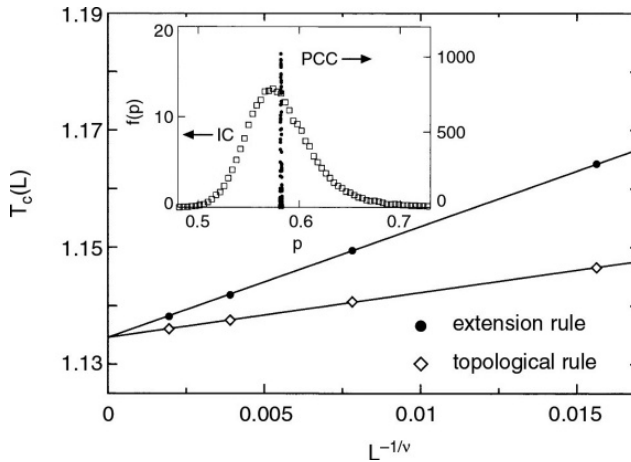
Fig. 5.3 Finite size scaling plot for the 'critical point' for $L \times L$ Ising square lattices. The inset shows the distribution of $p$, i.e. $f(p)$ for $L = 64$ for the probability changing (PCC) and invaded cluster (IC) algorithms. Note that a factor of 2 difference in the Hamiltonian produces a critical temperature that is only half as large as the 'usual' value. From Tomita and Okabe (2001).

algorithm (Machta *et al.*, 1995), combines features of invasion percolation (see Section 3.6.3) and cluster flipping to produce a method that has the property of 'self-organized criticality'. For the Ising model the algorithm proceeds as follows. Some initial spin configuration is chosen and all bonds connecting spins of the same type are assigned (independently) random numbers drawn uniformly in the interval between 0 and 1. Cluster growth proceeds by the systematic addition of the bond with the smallest random number, where every site is a 'seed', and terminates when the largest cluster 'spans' the system. Clusters of spins are then flipped with probability $\frac{1}{2}$, and the process begins anew. The fraction of the bonds accepted during the growth process approaches the percolation threshold $p_c$ as the lattice size approaches infinity and the critical temperature can then be extracted by inverting Eqn. (5.2). A cluster may be considered to span the lattice either when the maximum separation in one direction is equal to the lattice size $L$ (extension rule) or when the topological condition that the cluster has wound around the system in some direction (topological rule) applies. Relaxation times for this method are quite short, and it can be adapted for the study of both first order and second order phase transitions. The invaded cluster algorithm has also been successfully applied to systems with continuous degrees of freedom (Dukovski *et al.*, 2002).

### 5.1.6 Probability changing cluster algorithm

Tomita and Okabe (2001) have proposed a very clever algorithm which is based upon ideas of cluster flipping. The method extends the Swendsen–Wang method and uses a negative feedback mechanism to 'find' the critical temperature. The first stage of the algorithm is to use Swendsen–Wang sampling at some initial temperature to construct clusters by connecting spins

of the same type with probability $p = 1 - \exp(-2\mathcal{J}/k_B T)$ (see Eqn. (5.2)) and to 'flip' clusters accordingly. If the system is percolating, the probability $p$ is decreased by some small amount $\Delta p$, and if the system is not percolating, $p$ is increased by a small amount $\Delta p$. The new value of $p$ is used to construct new clusters and the process continues. The progress of the system is monitored and $\Delta p$ is decreased; as $\Delta p \to 0$ the estimate of $p_c$, and thus $T_c$, should become quite accurate. In Fig. 5.3 we show the results of the application of this approach to the two-dimensional Ising model (Tomita and Okabe, 2001). The finite size scaling behavior of the estimates for finite lattice $T_c$ extrapolates quite accurately to the exact value. The algorithm has also been successfully applied to a number of other systems including those with classical spins.

## 5.2 SPECIALIZED COMPUTATIONAL TECHNIQUES

### 5.2.1 Expanded ensemble methods

In many cases it is preferable to work in other ensembles, e.g. to include the temperature $T$ in the set of dynamic variables (i.e. in the Markov process a random walk is also carried out over a range of temperatures). These methods will be treated in some detail in the next chapter. In the remainder of this section we shall concentrate on specialized techniques that apply primarily to spin systems.

### 5.2.2 Multispin coding

Multispin coding is a name given to a variety of very closely related algorithms which pack multiple spins into a single computer word, and then, through the use of a control word, carry out the spin-flip acceptance or non-acceptance for all spins in the word simultaneously (Zorn *et al.*, 1981; Wansleben, 1987). The goal is to reduce both storage and CPU times, and the performance of multispin coding is very strongly machine dependent. Since all spins in a word will be considered in a single step, it is essential that they do not interact with each other. The checkerboard decomposition, described in Section 4.2.1, was developed explicitly for the purpose of implementing Monte Carlo on vector computers, and the use of a checkerboard decomposition is necessary for multispin coding on any computer. First, spins on a single sublattice are packed into 'multispin storage words' *is*. For an Ising model '$n$' spins may be packed into a single word, where the word length is '$n$' bits. For a $q$-state Potts model or other discrete state models, fewer spins may be packed into each word, depending on the number of bits needed to represent the possible spin states. The flipping probabilities are computed for each spin and compared with a random number creating a 'multispin flip word' *iscr* and spin flipping is then carried out by the exclusive or operation $is = iscr.XOR.is$. Sublattices are alternated in turn, and the resultant algorithm may yield substantial enhancement of performance.

In a variation of this method, which we refer to as 'multilattice coding', the same site from multiple, independent lattices is packed into a single word. Thus, for an Ising model '$n$' lattices may be packed into a word of '$n$' bits. Each lattice may be for instance at a different temperature. The advantage of this technique is that it offers the possibility of rapid production of data for '$n$' different, independent systems and hence the possibility of calculating error bars based upon '$n$' different runs. Since there is only one spin per system per word, there is no saving in memory.

While multispin coding speeds up the Metropolis algorithm significantly, it still suffers strongly from critical slowing down. Consequently, cluster algorithms are preferable for the study of bulk critical phenomena. However, for problems unrelated to bulk criticality (e.g. wetting phenomena, capillary condensation, etc., see Section 5.9 below) multispin coding still finds its place. See Bryk and Binder (2013) for a recent example in which systems as large as $512 \times 512 \times 36$ (i.e. more than 9 million spins!) were simulated, combining multispin coding and parallel tempering techniques (see Section 5.4.2).

### 5.2.3  *N*-fold way and extensions

The algorithms which we have discussed so far have been time-step-driven methods, i.e. they were based on following the development of the system at each tick of some fictitious clock. At very low temperatures the flipping probability becomes quite small and virtually nothing happens for a long time. In order to avoid this wasteful procedure Bortz *et al.* (1975) introduced an event-driven algorithm (the '$N$-fold way') in which a flip occurs at each step of the algorithm and one then calculates how many ticks of the clock would have elapsed if one had done it the 'old way'. They applied their method to the two-dimensional Ising model and we shall describe it now in terms of this system even though it can be applied to other discrete spin systems as well. In the literature this method has occasionally been termed 'kinetic Monte Carlo', but we will retain the usage of 'kinetic Monte Carlo' (KMC) to refer to sampling in which attempted moves must first overcome a thermal barrier and the resultant time dependence of the system differs from that in which only the initial and final states matter. This topic will be considered in more detail in Section 10.7.

We begin by recognizing that there are only a small number of possible local environments which a spin can possibly have and consequently a limited number of different flipping probabilities. One thus collects all spins in the system into lists, in which each member has the identical energetic local environment. For an Ising $S = 1/2$ square lattice, for a spin with $\sigma = +1$ there are only five possible arrangements of nearest neighbors with different energies, i.e. the number of neighbors which also have $\sigma = 1$ may only be 4, 3, 2, 1, or 0. The same number of possibilities exist for a spin $\sigma = -1$, so every spin in the system can belong to one of only 10 classes. (If next-nearest neighbor interactions are present or the system is three-dimensional the number of classes will be different, but in all cases it will be some modest size integer $N$. Hence the

name $N$-fold way.) The total probability of any spin of class $l$ being flipped in a given step is

$$p_l = n_l e^{-\Delta E_l / k_B T}, \tag{5.8}$$

where $n_l$ is the number of spins which are in class $l$. The integrated probability of 'some' event occurring in a given step for the first $M$ classes is simply

$$Q_M = \sum_{l \leq M} p_l. \tag{5.9}$$

Then $Q_N$ is the total probability for all $N$ classes. The procedure is then to generate a random number $0 < rn < Q_N$ to determine the class from which the next spin to be overturned will come, i.e. class $M$ is chosen if $Q_{M-1} < rn < Q_M$. Once the class has been chosen, another random number must be chosen to pick a spin from among those in the class. Finally, a third random number will be used to determine how much time has elapsed before this event has taken place, and we will discuss this part of the algorithm in a minute. First, we want to say a few words about bookkeeping. Each time a spin is flipped, it changes class. The site must then be removed from the list belonging to its original class and added to the new list corresponding to its new class. In addition, all of its (interacting) near neighbors change class. The key to an efficient $N$-fold way algorithm is thus an effective way of maintaining and updating the lists.

   In order to determine the 'lifetime' of a state we first consider the probability that the system is in state $\{\sigma\}$ at time $t$ and then undergoes a transition between time $t$ and time $t + \Delta t$:

$$\Delta P(t) = -P(t) \frac{Q_J}{\tau} \Delta t, \tag{5.10}$$

where $\tau$ is the time needed to execute a flip. The probability of a flip of a spin in any class is then

$$P(\Delta t) = \exp\left(-\frac{Q_J}{\tau} \Delta t\right). \tag{5.11}$$

Treating this as a stochastic process, we can generate a random number $R$ between 0 and 1, and inverting Eqn. (5.11), we find that the 'lifetime' of the state before flipping occurs becomes

$$\Delta t = -\frac{\tau}{Q_N} \ln R. \tag{5.12}$$

The thermodynamic averages of properties of the system are then calculated by taking the lifetime weighted average over the different states which are generated. The $N$-fold way is rather complicated to implement and each spin-flip takes a considerable amount of CPU time; however, at low temperatures, the net gain in performance can be orders of magnitude.

   A generalization of the $N$-fold way algorithm is the technique of 'absorbing Markov chains', or MCAMC (Novotny, 1995a), which offers substantial

additional advantage in looking at magnetization switching in nanoscale fer-
romagnets and related problems. At low temperatures a strongly magnetized
ferromagnet will not immediately reverse when a magnetic field is applied
in the opposite direction because the nucleation barrier to the formation of
a cluster of overturned spins is large. In a Monte Carlo simulation the same
problem occurs and very long times are needed to follow the magnetization
reversal process using standard techniques. The MCAMC approach extends
the $N$–fold way algorithm to allow the simultaneous flipping of more than one
spin to enhance the speed at which a nucleation cluster is formed; the 'level'
of the method determines how many spins may be overturned in a single step.
The level 1 MCAMC is essentially a discrete time version of the $N$–fold way
(Novotny, 1995b) and is best used for an initial state in which all spins are up,
i.e. for class 1 spins. A random number $R$ is picked and then the lifetime $m$
of the state is determined from $p_o^m < R < p_o^{m-1}$, where $p_o = 1 - p_1$. A spin
is then randomly chosen and overturned. Level 2 MCAMC offers a decided
advantage in the case that the nucleation cluster size is at least two, since it
avoids the tendency to flip back those spins that have just been overturned.
The level 2 MCAMC begins with a fully magnetized state and overturns two
spins; these may either be nearest neighbors of each other or may be more
distant neighbors which do not interact. Then one must define a transient sub-
matrix $T$ which describes the single time step transition probabilities, i.e. for
overturning one spin to reach a transient (intermediate) state, and the recur-
rent submatrix $R$ which gives the transition probabilities from the transient
to the absorbing (final) states. Again a random number $R$ is chosen and the
lifetime of the state is determined by $\mathbf{v}^T T^m \mathbf{e} < R < \mathbf{v}^T T^{m-1} \mathbf{e}$ where $\mathbf{v}$ is the
vector describing the initial state and $\mathbf{e}$ is the vector with all elements equal
to one. Another random number is then generated to decide which spins will
actually flip. Following generation of the 'initial cluster' as just described, the
$N$–fold way may then be used to continue. This method may be systematically
extended to higher order when the size of the nucleation cluster is larger so
that the process of overturning a cluster is 'seeded'. It is also possible to use
the concept of spin classes to devise another algorithm that can bridge the
disparate time and length scales desired in Monte Carlo simulations (Kolesik
*et al.*, 1998).

An interesting, adaptive algorithm proposed by Adam *et al.* (1999) inter-
polates between a kinetic Metropolis algorithm and the $N$–fold way method.
In their kinetic Metropolis method the time steps are not constant but have an
exponential dependence upon random numbers. Nonetheless, there is still a
rejection probability. The adaptive algorithm begins with the kinetic Metrop-
olis algorithm but stores the transition probabilities of rejected transitions in
order to use them later. If the transition is accepted, another kinetic Metrop-
olis transition is attempted. Otherwise, a new attempt configuration is selected
randomly from the other available choices and the process is repeated. The
advantage of this approach is that only a single transition probability is needed
for each attempt, and if the rejection probability is low the method is efficient.
If the rejection rate is high, however, the algorithm begins to resemble the
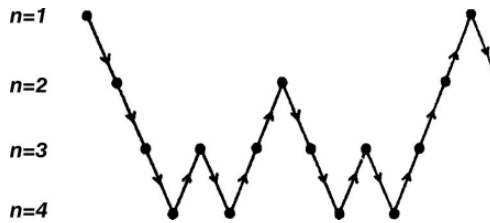$N$–fold way.

Fig. 5.4 Schematic description of a multigrid Monte Carlo cycle. The degree of blocking is given by $n$ so that the size of the 'blockspin' lattice is $L/b^n$ where the size of the blocking is denoted by $b$.

**Problem 5.3** Perform an $N$-fold way of a $32 \times 32$ Ising square lattice with periodic boundary conditions at $T = 1.5 \, J/k_B$. Determine the results for the internal energy and the correlation time for the internal energy and compare the answers with the corresponding results for a Metropolis simulation at this temperature. Repeat this comparison for $T = 0.5 \, J/k_B$.

### 5.2.4 Hybrid algorithms

In this section we consider methods which employ a combination of different algorithms. The goal of this approach is to take advantage of the characteristics of each component algorithm to produce a method which is superior to each individually. Microcanonical algorithms generate new states very rapidly, but all states are confined to a constant energy surface (see e.g. Creutz, 1980). By mixing Metropolis and microcanonical algorithms, one produces a technique which is ergodic and canonical. Also the mixing of Monte Carlo and molecular dynamics algorithms goes under the name 'hybrid Monte Carlo', but this will be discussed in Chapter 12, Section 12.2.4.

### 5.2.5 Multigrid algorithms

Multigrid methods are an alternative approach to the reduction of critical slowing down. 'Blocks' of spins of various sizes are considered at different time steps and all the spins within a given block are either flipped or not in a sort of coarse-graining procedure. The change in block size is done in a systematic fashion, and examples are shown in Fig. 5.4. While multigrid Monte Carlo (Kandel *et al.*, 1988; 1989) can be shown to eliminate critical slowing down perfectly for continuous spin models where the single-site probability is a Gaussian, the method is already less successful for cases where the single site probability is a $\phi^4$ model (Goodman and Sokal, 1986) or for models with discrete spins. Thus we do not describe this method further here.

### 5.2.6 Monte Carlo on vector computers

The use of vector computers for Monte Carlo calculations has been immensely successful; and even though everyone anticipates the dominance of parallel computing in the future, in many cases vector computing is still the most efficient and user friendly computing tool. Compilers on vector computers

tend to be quite mature and rather efficient code can thus be produced without enormous user effort. The basic idea of vector computing is to speed up computation by arranging the problem so that essentially the same operation can be performed on an entire vector of variables which is loaded into the 'vector pipe' at the start. This necessitates program construction which insures that all elements of the vector are independent and that the change of one does not affect any other. For a Monte Carlo calculation on a simple lattice model, the checkerboard decomposition discussed in Chapter 4 achieves this goal. For more details on implementation of Monte Carlo programs and application examples we refer to a separate review (Landau, 1992). Certainly a familiarity with vector computing provides, at the very least, a better understanding of the issues raised in over a decade of the literature.

In the early 1990s, vector computing began to fall out of favor (at least machines for which the user would explicitly write code in vector format) in the United States because of the perception that parallel computers would offer substantial performance–cost ratio improvement. The appearance of the 'Earth Simulator' in Japan suggested that vector computing might still have a significant role to play in scientific computing. This machine is a parallel–vector supercomputer jointly built by the Earth Simulator Research and Development Center (ESRDC, predecessor of ESC) and NEC (costing $350–400 million). This unique system architecture produces enough power to solve the complex scientific calculations used in climate and crustal modeling and reaches approximately 40 Tflops peak performance. Whereas the Earth Simulator was the most powerful machine that had yet been built at the time of writing of the second edition of this book, now, less than a decade later (September 2013), it is not even on the list of the Top 500 Supercomputers! The fastest machines now available are the massively parallel Tianhe-2 in China with 3 120 000 cores (combining Xeon and Xeon Phis) and a peak performance of 54.9 petaflops. The second fastest is Titan at ORNL in the USA with 560 640 cores (combining Opterons and NVIDEA GPUs) and a peak performance of 27.1 petaflops, followed in third place by a Blue Gene/Q at LLNL in the USA with 1 572 864 cores and a peak performance of 20.1 petaflops. The fourth place machine, the Japanese K Computer at RIKEN Advanced Institute for Computational Science, has 705 024 cores and a peak performance of 11.3 petaflops. The tendency to move towards hybrid, massively parallel machines is clear, and this characteristic makes efficient programming increasingly difficult. In fact, several installations declined to submit new performance numbers to the last Top 500 Supercomputer list because they felt that the effort needed to optimize LINPACK could be better devoted to doing computational science!

### 5.2.7 Monte Carlo on parallel computers

One of the most effective uses of parallel architectures is to simply perform independent Monte Carlo simulations of a system under different conditions on different processors. This approach, called 'trivial parallelism', is obviously not the goal of designers of these machines, but is often the most effective from the user point of view. For very large problems, parallel architectures offer

the hope of speeding up the simulation dramatically so that data are produced within a reasonable turnaround time. Broadly speaking, parallel algorithms may be of two different types. The work to be done on a system may be spread among multiple processors, or the system may be decomposed into different parts and each processor may be assigned to work on a different part of the system. This latter approach is almost always more effective if a substantial number of processors is available. Simple lattice systems may be split up into squares or strips. For systems with continuous positional degrees of freedom, one may either assign a fixed region of space to a processor or a fixed set of particles. The determination of which approach is more efficient depends on the characteristics of the problem at hand. For example, for systems with very strong density fluctuations, a rigid spatial decomposition of the problem may result in some processors having the responsibility for many particles and others having no work to do within a given time interval. One particularly important consideration in the development of any type of parallel program is the relative importance of communication time and computation time. In the case of geometric parallelization, i.e. decomposition of a system into strips, if the size of the individual regions is too small, the time used to communicate information between processors may not be small compared to the time needed on each processor for computation. In such a case, the performance may actually get *worse* as processors are added (Heermann and Burkitt, 1990). For systems with long range interactions (e.g. spin systems with exchange constants which decay with distance according to a power law) most of the computational effort goes into the calculation of energy changes, and then the communication overhead is much less of a problem.

The clever use of parallel algorithms continues to enhance the performance of Monte Carlo simulations and this tendency is unlikely to abate soon. Although more detailed descriptions of parallel implementation are beyond the scope of this text, additional information is already abundant; see, e.g., Heffelfinger (2000) and Uhlherr (2003). At the time of this writing, petaflop computers have already been used for Monte Carlo research simulations: the 2009 ACM Gordon Bell prize was awarded to a group from ORNL who developed a parallel WL–LSMS (Wang–Landau locally self-consistent, multiple scattering) code that ran at 1.8 petaflops on the Jaguar supercomputer (Eisenbach *et al.*, 2009). While some predictions are clearly speculative, it is clear that the pace of increase in performance is not abating and that the 'power user' will have to become proficient in the efficient development of codes for a large number of processors. This represents a significant challenge since many parallel implementations to date begin losing efficiency at $\sim 100$ processors.

## 5.3 CLASSICAL SPIN MODELS

### 5.3.1 Introduction

There are many important lattice models in statistical mechanics which do not have discrete degrees of freedom but rather variables which vary continuously.

Just as the Ising model is the 'standard' example of a discrete model, the classical Heisenberg model is the most common prototype of a model with continuous degrees of freedom. A more general model which includes the Heisenberg system as a special case involves classical spin vectors $\mathbf{S}_i$ of unit length which interact via a Hamiltonian given by

$$\mathcal{H} = -\mathcal{J} \sum_{i,j} \mathbf{S}_i \cdot \mathbf{S}_j - D \sum_i \mathbf{S}_i^2, \qquad |\mathbf{S}_i| = 1, \qquad (5.13)$$

where the first term is the Heisenberg exchange interaction and the second term represents single ion anisotropy. This Hamiltonian describes many physically interesting magnetic systems, and even examples of $D = 0$ have been experimentally verified for magnetic ions with large effective spin values, e.g. $RbMnF_3$. We must remember, of course, that at sufficiently low temperatures the classical Hamiltonian cannot be correct since it neglects quantum mechanical effects (see Chapter 8). In the remaining parts of this section we shall consider methods which can be used to simulate the Heisenberg model and its anisotropic variants. Much of what is said here can be carried over to lattice models of liquid crystals as well, where one may use a Hamiltonian similar to Eqn. (5.13) but with the spin vector replaced by a tensor describing the orientational degrees of freedom of an elongated or disk-like molecule.

In the systems with discrete degrees of freedom that have been discussed earlier, the elementary excitations cost a finite amount of energy and the thermodynamic properties tend to be dominated by exponential decays at low temperature. In contrast, systems described by Hamiltonians with classical spins, e.g. Eqn. (5.13), will have excited states that cost an infinitesimal amount of energy. Thus, elementary excitations generally can be described by simple harmonic oscillators at quite low temperatures and the equipartition theorem can be used to determine low temperature properties. For a system with three-dimensional spins, i.e. $\mathbf{S} = (S_x, S_y, S_z)$ with fixed length spins $|\mathbf{S}| = 1$, the low temperature specific heat will be given by $C/N = 2 \times \frac{1}{2} \times k_B$. If one of the spin components is completely quenched, the specific heat would be suitably reduced, i.e. $C/N = 1 \times \frac{1}{2} \times k_B$. Since Monte Carlo methods tend to have difficulties at low temperatures because of 'thermal sluggishness', a comparison with the predicted equipartition value is a good way to check on whether or not the system has reached equilibrium.

### 5.3.2  Simple spin-flip method

The Metropolis method can be used for Monte Carlo simulations of classical spin vectors if we allow a spin to 'tilt' towards some new direction instead of simply flipping as in an Ising model. In the simplest approach, some new, random direction is chosen and the energy change which would result if this new spin orientation is kept is then calculated. The usual Metropolis prescription is then used to determine, by comparison with a random number generated uniformly in the interval [0, 1], whether or not this new direction is

accepted, i.e. the transition rate is

$$W_{n \to m} = \tau_o^{-1} \exp(-\Delta E / k_B T) \qquad \Delta E > 0 \qquad (5.14a)$$
$$= \tau_o^{-1} \qquad\qquad\qquad \Delta E < 0, \qquad (5.14b)$$

where $\Delta E$ is simply the energy difference between the initial and trial state. When beginning such a simulation one must first make a decision about whether information about the spins will be kept by keeping track of Cartesian spin components or by keeping track of angles in spherical coordinates. The manipulation of spins in angular coordinates is usually quite time consuming, and it is generally more efficient to use Cartesian coordinates. (One price which one must then pay is that the spin length is no longer fixed to remain exactly equal to unity.) A new spin direction can then be chosen by randomly choosing new spin components and normalizing the total spin length to unity. The simplest way to accomplish this is to generate a new random number in the interval [0, 1] for each component and then subtract 0.5 to produce components such that $-0.5 < S_\alpha < 0.5$; by normalizing by the length of the spin one obtains a new spin of length unity. If this procedure is used, however, the spins are not part of a uniform distribution of directions since they are more likely to point towards the corners of a unit cube than in other directions. Instead, one must first discard any new spin which has a length greater than 0.5 before renormalization, but if this is done, the new spins will be uniformly distributed on the unit sphere. An interesting alternative procedure was suggested by Marsaglia (1972). Two random numbers $r_1$ and $r_2$ are chosen from a uniform distribution to produce a vector with two components $\zeta_1 = 1 - 2r_1$ and $\zeta_2 = 1 - 2r_2$. The length of the vector is determined by $\zeta^2 = \zeta_1^2 + \zeta_2^2$ and if $\zeta^2 < 1$ a new spin vector is then computed with components

$$S_x = 2\zeta_1(1 - \zeta^2)^{1/2}, \quad S_y = 2\zeta_2(1 - \zeta^2)^{1/2}, \quad S_z = 1 - 2\zeta^2. \quad (5.15)$$

Note that this procedure is *not* simply the generation of points randomly in the unit circle and then projecting them onto the unit sphere since this would not produce a uniform distribution. Any of the methods for producing new trial spin configurations require multiple random numbers, moreover the continuous variation of possible energies eliminates the possibility of building a table of probabilities. Thus, continuous spin models are much more time consuming to simulate. (A trick which can be used is to approximate the possible spin directions by a discrete distribution, e.g. for a two–dimensional XY-model one could use an $n$-state clock model with the spins confined to point in one of $n$ different equally spaced directions. The discreteness which results would then allow table building; however, it may also modify the behavior. At low temperatures, for example, the effective anisotropy introduces a gap into the excitation spectrum which is not present in the original model. In two–dimensional models the nature of the phase transitions is also modified. Thus, even though such approaches may improve performance, they must be treated with caution.)

One additional feature that needs to be discussed is the choice of an order parameter. These systems now have order parameters with multiple components, and the nature of the Hamiltonian determines just which components are important. In the case of single ion anisotropy ordering will occur only along the $z$-direction so this component must be kept track of separately from the other components. In the fully isotropic case, all components are equivalent. The order parameter is then invariant under global rotation so it is the magnitude of the order parameter which matters, i.e.

$$ m = \sqrt{M_x^2 + M_y^2 + M_z^2}, \quad \text{where } M_\alpha = \frac{1}{N} \sum_i S_{i\alpha}. \qquad (5.16) $$

In this case the order parameter can never be zero, even above $T_c$, so finite size effects are always quite pronounced. The usual fluctuation definition of the susceptibility is also no longer valid although it can be used as an 'effective' susceptibility. Above $T_c$ the best estimate for the true susceptibility is simply

$$ \chi = \frac{N}{k_B T} \langle m^2 \rangle \qquad (5.17) $$

since $\langle m \rangle$ will be zero in the thermodynamic limit.

**Problem 5.4** Perform a Metropolis simulation of a $8 \times 8 \times 8$ classical Heisenberg model on a simple cubic lattice with periodic boundary conditions at $T = 2.0 \ J/k_B$ and $T = 4.0 \ J/k_B$. Determine the internal energy and order parameter. Comment on your findings.

### 5.3.3 Heatbath method

A variation of this method which was first suggested for application to lattice gauge theories (see Chapter 11) corresponds to touching each spin in turn (selected either in order or randomly) to a 'heatbath' (Creutz, 1980). Instead of allowing the change in energy to determine the 'new' spin configuration, one can simply randomly select a new spin direction and then compare a random number $rn$ with the Boltzmann probability of the trial configuration, i.e. accept the new configuration if $rn < \exp(-E'/k_B T)$, where $E'$ is the energy of the trial state. This method is most useful in circumstances where the Metropolis-like approach described above has a very low acceptance rate. In simulations of lattice gauge models the determination of the energy of a given state may be very time consuming so one may repeat the heatbath process many times, with the same new trial state, and use the collection of configurations which result for the statistical averaging. The entire process must be repeated many times, and after equilibration has occurred, many Monte Carlo steps must be made to obtain good statistical averaging. The heatbath method may also be used for Ising model simulations for which there are only two different states for each

spin. Here the spin may be set equal to $+1$ with probability $p_i$ and equal to $-1$ with probability $1 - p_i$ where

$$p_i = \frac{e^{2\beta \sum_{nn} \sigma_j}}{1 + e^{2\beta \sum_{nn} \sigma_j}}. \tag{5.18}$$

This may be easily implemented by generating a random number $rn$ and setting

$$\sigma_i' = \text{sign}(p_i - rn). \tag{5.19}$$

Note that the probability of a spin being up or down is the same for Glauber dynamics, however, the implementation is different since

$$\sigma_i' = \text{sign}(rn - (1 - p_i)) \qquad \text{if } \sigma = +1, \tag{5.20a}$$
$$\sigma_i' = \text{sign}(p_i - rn) \qquad \text{if } \sigma_i = -1. \tag{5.20b}$$

This means that the random numbers are used differently and the actual sequence of states will be different (Herrmann, 1990).

### 5.3.4 Low temperature techniques

#### 5.3.4.1 Sampling

In classical spin systems there is no gap in the excitation spectrum. Very low energy excitations dominate at low temperatures, but a random choice of new spin direction will generally produce a large energy change and is thus unlikely to be accepted. The acceptance rate can be increased by restricting the new spin–flip attempts to a small cone about the initial position. If the cone is made too narrow, however, the changes are so small that the system again evolves quite slowly. Hence some initial trials followed by an intelligent choice of the angle for the cone of maximum displacement must be made.

#### 5.3.4.2 Interpretation

At low temperatures the excitations are spin waves which can be most readily explained by a harmonic analysis in reciprocal (momentum) space. For small lattices, however, the reciprocal space is quite coarse-grained and the number of momentum points $\mathbf{q}$ is limited. Thus, finite size effects can become important, not because of any critical behavior but because of the restrictions on the number of modes.

### 5.3.5 Over-relaxation methods

Strictly speaking over-relaxation (Brown and Woch, 1987; Creutz, 1987) techniques are deterministic, but they are of great value when used in combination with other, stochastic approaches. The effective interaction field for a spin is determined by examining all neighbors to which it is coupled. The spin is then

precessed about this interaction field by an angle $\theta$, making use of the equation of motion

$$\dot{\mathbf{S}} = -\mathbf{S} \times \mathbf{H}_{\text{eff}}. \qquad (5.21)$$

This process is microcanonical since the energy is a constant of the motion, but for large values of $\theta$ it can enhance decorrelation. If a checkerboard algorithm is used, every spin on a single sublattice may be considered, and then each spin on the next sublattice treated. This algorithm is deterministic, but when used together with a stochastic technique, e.g. Metropolis, the resultant states are drawn from a canonical ensemble. This method is quite efficient and vectorizes extremely well.

### 5.3.6 Wolff embedding trick and cluster flipping

At first glance the cluster flipping methods which have been described earlier would seem to be restricted to systems with discrete states, but Wolff (1989a, 1989b) has also shown how these methods can be applied to general $O(n)$ models (i.e. $n$-component vector models). This approach, known as the embedding trick, turns the original uniform interaction classical spin model into an Ising model with inhomogeneous couplings. It proceeds in the following manner. First a direction $\hat{n}$ is chosen randomly in space. The spins are then projected onto that direction to form an Ising model with interactions between pairs which depend on the projections of each spin. In principle the Metropolis method could then be used to flip spins, but it is clearly more effective to use a cluster flipping method. If the single cluster (Wolff) flipping algorithm is to be used, bonds are added between nearest neighbor sites with probability

$$p = 1 - \exp\{\min[0, 2\beta \mathcal{J}(\hat{n} \cdot S_i)(\hat{n} \cdot S_j)]\} \qquad (5.22)$$

to form a connected cluster of sites in the same way as for a simple Ising model. The components parallel to $\hat{n}$ are then reversed for every spin in the cluster to yield a new spin configuration. Note that in this case the projection need only be carried out for those spins which have a chance to join the cluster to be flipped. A new direction is randomly chosen in space and the process is repeated. Data are collected in the usual way. (See also Section 5.1.3 in this chapter for a quick review of the cluster flipping technique for the Ising model.)

We wish to emphasize that this trick is not just of academic interest since it has already been used to extend the studies of critical phenomena in classical spin systems well beyond what was previously possible. For example, a very successful investigation of the three-dimensional, classical, Heisenberg model has been made using the embedding trick Wolff flips together with histogram reweighting (see Chapter 7) and a finite size scaling analysis to determine the critical temperatures on several lattices with quite high precision (Chen *et al.*, 1993). Lattices as large as $40 \times 40 \times 40$ with periodic boundary conditions were simulated with the results: $\mathcal{J}/k_{\text{B}} T_{\text{c}} = 0.693\,035(37)$ (body centered cubic lattice with two atoms per unit cell) and $\mathcal{J}/k_{\text{B}} \ T_{\text{c}} = 0.486\,798(12)$ (simple cubic lattice). The critical exponents were found with high precision and the

values agreed quite closely for the two lattices in full support of our ideas of universality. A Wolff cluster study of this system by Holm and Janke (1993) yielded similar results but with less resolution. Whereas these lattice sizes are still much smaller than those which are accessible for the Ising model, they represent a dramatic improvement over what could be treated by Metropolis sampling. Other systems have been studied with this method as well. The three-dimensional XY-model (plane rotator) was studied by Hasenbusch and Meyer (1990) using the Swendsen–Wang cluster update method together with the embedding trick and improved estimators. They found a critical coupling of $\mathcal{J}/k_B T_c = 0.454\,21(8)$ and obtained estimates for static and dynamic critical exponents from finite size scaling. All of the above mentioned studies indicate that the combination of several methods, for both simulation and analysis, can indeed be quite powerful.

**Problem 5.5**  Using the embedding trick perform a Wolff cluster simulation of a $8 \times 8 \times 8$ classical Heisenberg model on a simple cubic lattice with periodic boundary conditions at $T = 2.0\ J/k_B$. Determine the internal energy and order parameter and compare the results with those of Problem 5.4.

### 5.3.7 Hybrid methods

Often it is advisable to combine different updating schemes into a single, more complicated scheme that is more efficient in destroying correlations between subsequently generated states on all length scales. Thus, it is straightforwardly possible to mix ordinary Metropolis or heatbath sweeps through the lattice with Wolff cluster flips, etc. A very successful study of the two-dimensional classical, XY-model (three component) used a mixture of Metropolis, over-relaxation and embedding trick Wolff flips together with a finite size scaling analysis to determine the Kosterlitz–Thouless temperature to much higher precision than had previously been possible (Evertz and Landau, 1996), $\mathcal{J}/k_B T_{KT} = 0.700(5)$.

Another technique which is actually termed 'hybrid Monte Carlo' has been used in lattice gauge theories (see Chapter 11) but is also straightforward to implement for classical spin systems. Instead of choosing the trial configuration by random change of a single spin (or link for lattice gauge models) one can instead produce a trial state by changing all spins by a small amount determined from the canonical equations of motion. (Such time integration methods will be discussed in Chapter 12. As a note, we add that a symplectic integrator is best chosen to insure detailed balance. For lattice gauge models it may be necessary to introduce fictitious momenta in order to accomplish this.) The acceptance or rejection of the new trial state can then be made via standard Metropolis.

### 5.3.8 Monte Carlo dynamics vs. equation of motion dynamics

In the previous sections we have discussed a number of techniques which allow us to 'speed up' the Monte Carlo sampling through phase space through the intelligent choice of 'step' size and direction. For some systems such changes

can be made with impunity since the time development of the system being modeled is stochastic. In some cases systems have true dynamics which are described by Poisson's equations if they are classical or by the commutator if they are quantum, i.e.

$$\dot{S}_i = -\frac{i}{\hbar}[\mathcal{H}, S_i], \tag{5.23}$$

where $\mathcal{H}$ is the Hamiltonian and $S_i$ the operator in question. Equation (5.23) represents an equation of motion and takes the system along a deterministic path through phase space. This path has physical significance and the associated time is true time. In contrast, the Monte Carlo method is strongly dependent on the (arbitrary) transition rate which is chosen. For the Ising model, Eqn. (5.23) yields no equations of motion since the commutator is zero. The Ising model thus has only stochastic 'dynamics', i.e. kinetics. The time-dependent behavior of the Heisenberg model may be studied either by Monte Carlo kinetics or by integrating deterministic equations of motion obtained through Eqn. (5.23); the time-dependent critical behavior will be different in the two cases (Landau, 1994; Landau and Krech, 1999).

### 5.3.9 Topological excitations and solitons

In most situations discussed so far, deviations from the groundstate are produced by spin-flips or by periodic, spin-wave excitations. In some cases, other kinds of excitations have fundamental importance. In the two-dimensional XY-model, in addition to spin waves, topological excitations known as vortices play a crucial role. The vortex cores can be located by following the spin directions around an elementary plaquette and summing the differences in the relative spin angles with regard to some fixed direction. If the sum is $2\pi$ a vortex is present, if the sum is $-2\pi$ an antivortex is present, and if the sum is 0 then no topological excitation is centered on the plaquette. Both spin waves and vortices are portrayed schematically in Fig. 5.5. At low temperatures a few tightly bound vortex–antivortex pairs are present in the two-dimensional XY-model, and as the temperature is increased the pairs unbind, signaling a special kind of phase transition. A Monte Carlo simulation does not manipulate the vortices directly since it is the spin degrees of freedom which are sampled, but the vortex behavior can be monitored along with the thermodynamic properties.

There are also slightly more complex systems which show a combination of order parameter fluctuations as well as topological excitations. As a simple 'case study' example we consider the two–dimensional Heisenberg antiferro-magnet with exchange anisotropy in a magnetic field,

$$\mathcal{H} = \mathcal{J}\sum_{\langle i,j \rangle}[(1-\Delta)(s_{ix}s_{jx} + s_{iy}s_{jy}) + s_{iz}s_{jz}] + H_{\parallel}\sum_i s_{iz}, \tag{5.24}$$

where $\mathcal{J} > 0$ is the antiferromagnetic nearest neighbor exchange parameter, $\Delta$ describes the exchange anisotropy, and $H_{\parallel}$ is an applied magnetic field in the $z$-direction. Data were obtained for this model using quite simple Monte Carlo

Fig. 5.5 Schematic
view of excitations in
classical spin models:
(a) spin waves;
(b) vortices in a
two–dimensional
plane; (c) solitons in a
one-dimensional
lattice with a
symmetry breaking
field.



(a)

wavelength λ          λ

spin wave

(b)

← core →

vortex          anti vortex

(c)

soliton
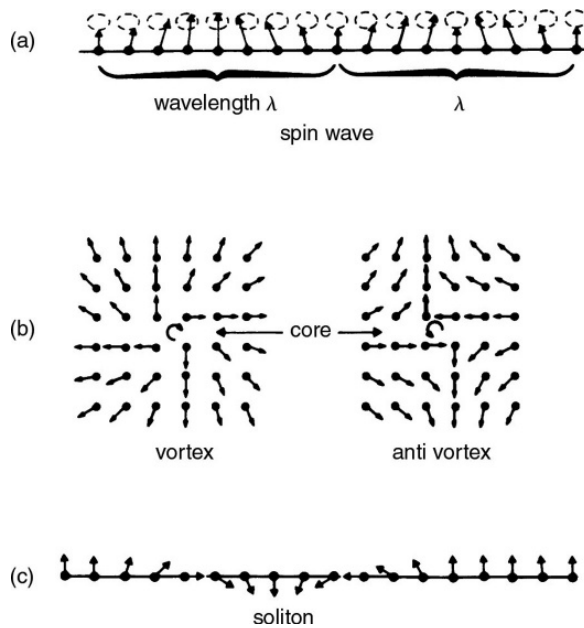
methods by Landau and Binder (1981) either by varying the temperature at fixed field strength or by sweeping the field at constant temperature. $L \times L$ lattices with periodic boundaries were simulated using the Metropolis method. From a combination of data on order parameters, magnetization, internal energy, susceptibility, and specific heat, a phase diagram was extracted in $H_{\parallel} - T$ space. This diagram, see Fig. 5.6, shows that in low fields below a field-dependent critical temperature, there is an Ising transition to a state in which the system shows antiferromagnetic order along the field direction. At high fields the $z$-components of the spins are aligned (but disordered) and only the $x$- and $y$-spin components are free to order. This is the so-called 'spin-flop' (SF) phase. However, since the symmetry is then the same as for a two–dimensional XY-model, we expect a Kosterlitz–Thouless transition with the formation of bound, topological excitations as the temperature is lowered. In three dimensions the upper and lower phase boundaries would meet at a Heisenberg-like bicritical point at some finite temperature, but in two dimensions the Heisenberg model does not order at any finite temperature so we would expect on theoretical grounds that they would meet at $T = 0$. The simulations show that these two phase boundaries come very close together, but it is not possible to determine whether or not they merge at some non–zero temperature. In the 'XY-like' phase, bound vortex–antivortex pairs are seen at low temperatures; in addition to increasing in density as the temperature is elevated, they begin to unbind, as is shown in Fig. 5.7a. The measured density is consistent with a non-zero excitation energy and the value of the 'gap' varies systematically with the applied field (see Fig. 5.7b). Of course, with modern computers and techniques one could obtain far better data on larger systems,
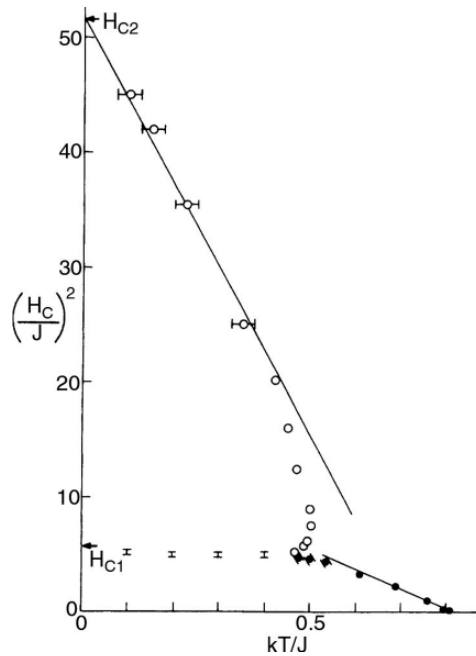
Fig. 5.6 Phase
diagram for the
two–dimensional
anisotropic
Heisenberg model (see
Eqn. (5.24)). From
Landau and Binder
(1981).

but even these results which require quite modest computer resources clearly
reveal the essential physics of the problem.

Another very intriguing situation is found in one–dimensional XY-models
with a symmetry breaking field. In the simplest possible case there may be
topological excitations in which the spins go through a $2\pi$-twist as we move
along the chain direction. This may be observed by simply monitoring the
angular position of successive spins. These excitations are known as solitons,
or, more properly speaking, solitary waves, and may exist in a variety of forms
in magnetic models. (See Fig. 5.5 for a schematic representation of a soliton
excitation.) For example, in an antiferromagnet each sublattice may rotate
through $\pi$ to form a new kind of soliton. It is also possible for one sublattice
to rotate through $\pi$ and the other sublattice to rotate through $-\pi$. In a third
variant, one sublattice is unchanged and the other rotates through $2\pi$: All of
these types of solitons have been observed in Monte Carlo simulations.

## 5.4 SYSTEMS WITH QUENCHED RANDOMNESS

### 5.4.1 General comments: averaging in random systems

By quenched randomness we imply that the model Hamiltonian of interest
depends on random variables other than the degrees of freedom which are
considered in the thermal average, and these random variables are kept fixed in
one physical realization of the system. For example, consider a magnetic binary

Fig. 5.7 Topological excitations in the two–dimensional anisotropic Heisenberg model. (a) 'Snapshots' of vortex behavior in the SF state for $L = 40$, $H_{\parallel}/J = 4.0$. Open and closed circles represent vortices and antivortices, respectively. (b) Vortex–pair density in the SF state. The energy (in units of $J$) needed to create a vortex–antivortex pair is $2\mu$. From Landau and Binder (1981).
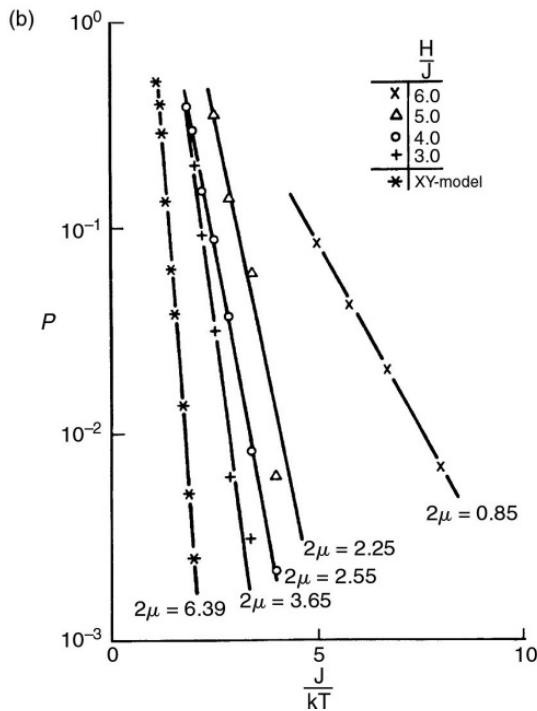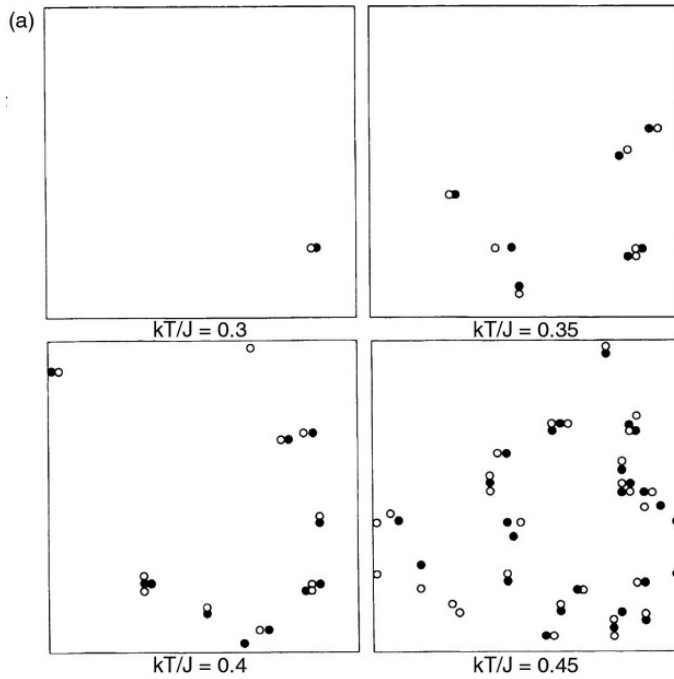
alloy $A_x B_{1-x}$, where a crystal is grown from a melt containing a fraction $x$ of A-atoms and a fraction $1 - x$ of B-atoms. Assuming that both species carry Ising spins $S_i = \pm 1$, it is nevertheless natural to assume that the exchange constants $\mathcal{J}_{ij}$ depend on the type of pair that is considered: $\mathcal{J}_{AA}$, $\mathcal{J}_{AB}$, or $\mathcal{J}_{BB}$, respectively. Denoting the occupation variable $c_i = 1$ if site $i$ is taken by an A–atom, $c_i = 0$ if it is taken by a B–atom, one would arrive at the Hamiltonian (assuming nearest neighbor exchange only)

$$\mathcal{H}\{S_i, c_i\} = -\sum_{\langle i,j \rangle} \{c_i c_j \mathcal{J}_{AA} + [c_i(1 - c_j) + c_j(1 - c_i)]\mathcal{J}_{AB}$$
$$+ (1 - c_i)(1 - c_j)\mathcal{J}_{BB}\} S_i S_j. \tag{5.25}$$

Of course, this model includes the dilution of a magnetic crystal by a non-magnetic species as a special case (then $\mathcal{J}_{AB} = \mathcal{J}_{BB} = 0$). While the configurations of the spins $\{S_i\}$ in all averages are weighted with the Boltzmann factor $\exp[-\mathcal{H}\{S_i, c_i\}/k_B T]$ in all averages, the configurations of the $\{c_i\}$ are not assumed to occur with a weight given by the Boltzmann factor, but rather with a predetermined distribution $P\{c_i\}$. Depending on the history of sample preparation in the laboratory, one may wish to choose the $c_i$ completely at random, but consistent with the chosen concentration $x$, or with some built-in correlations reflecting 'chemical' short range order. In any case, an average of some observable $A\{S_i, c_i\}$ (e.g. the magnetization $M$ of crystal) then becomes

$$[\langle A\{S_i, c_i\} \rangle_T]_{av} = \int d\{c_i\} P\{c_i\} \frac{1}{Z\{c_i\}} \underset{\{s_i\}}{\mathrm{Tr}}\, A\{S_i, c_i\} \exp[-\mathcal{H}\{S_i, c_i\}/k_B T].$$
$$\tag{5.26}$$

Thus one sees there is a double average that needs to be carried out: for a fixed realization $\{c_i\}$, one computes the thermal average as usual, and then this average is averaged once more with $P\{c_i\}$. While the thermal averaging is done with the usual Metropolis importance sampling, the disorder average $[\ldots]_{av} = \int d\{c_i\} P\{c_i\} \ldots$ can immediately be realized by simple sampling.

In principle, this problem is hence straightforwardly suitable for Monte Carlo simulation. However, the question arises how large the sample has to be for the averaging with $P\{c_i\}$ over the configurations $\{c_i\}$ of the quenched disorder variables. In an experiment, typically measurements are carried out for a single probe, there is no need to repeat the experiment for a large number of samples, the observable quantities are 'self-averaging'. One would expect that a similar self-averaging property would also apply to simulations, if very large systems away from any phase transition are studied, and then simulation of a single (or a few) realizations of the $\{c_i\}$ would suffice. However, the situation is rather different in the case of a finite size scaling analysis, where one considers systems of finite linear dimension $L$ right at the critical temperature $T_c$ of the model: the fluctuations from one sample $\{c_i\}$ to the next one cause a significant sample-to-sample fluctuation of the effective pseudo-critical temperature $T_c(L)$ of the system (defined e.g. by the maximum of the specific heat or the maximum slope of the fourth order cumulant, etc.). This

sample-to-sample fluctuation of $T_c(L)$ causes a lack of self-averaging for certain quantities (typically for the order parameter and its susceptibility) at $T_c$. This lack of self-averaging shows up when one considers ratios such as (Wiseman and Domany, 1995)

$$R_A \equiv [(\langle A \rangle_T - [\langle A \rangle_T]_{av})^2]_{av}/([\langle A \rangle_T]_{av})^2. \qquad (5.27)$$

Lack of self-averaging implies that ($\xi$ is the correlation length)

$$R_A \to C_A \quad \text{if} \quad L/\xi \to 0 \text{ (i.e. for } T = T_c) \qquad (5.28)$$

while away from $T_c$ there is self-averaging, ratios such as $R_A$ decay for $L \to \infty$ inversely proportional to the volume,

$$R_A \propto (\xi/L)^d \qquad \text{if } L \gg \xi. \qquad (5.29)$$

The lack of self-averaging implies that a sample of the order $n \approx 10^4$ realizations is desirable, in order to get the relative error of the disorder average at $T_c$, $[\langle A \rangle_{T_c}]_{av}$, down to 1% or less. This consideration already shows that the Monte Carlo study of phase transitions in random systems may be very computer time consuming. Of course, sometimes a relative error of 10% may seem acceptable, and then only a sample of $n \approx 10^2$ realizations is required.

In addition, one has to be careful in the precise manner in which the disorder averaging is carried out. Suppose we consider the case $c = 0.5$ for the $A_xB_{1-x}$ alloy. We can generate a sample $\{c_i\}$ by drawing a random uniformly distributed number $\eta_i$ with $0 \leq \eta_i < 1$ for each lattice site, and choosing $c_i = 1$ if $\eta_i > x$ and otherwise setting $c_i = 0$. However, for a crystal with $N = L^d$ sites the average composition will differ from $x = 0.5$ also by a random deviation of order $1/\sqrt{N}$. Since often dependence of the critical temperature $T_c(x)$ on concentration $x$ is rather strong, this sample-to-sample variation of the concentration may contribute substantially to the sample-to-sample fluctuation of the pseudo-critical temperature $T_c(L)$. However, this problem is avoided if one simply selects $N_x = xN$ lattice sites at random, setting $c_i = 1$ at each of these sites and otherwise putting $c_i = 0$. Then the concentration of every sample is strictly equal to $x$, and the sample-to-sample fluctuation of the concentration is suppressed. It turns out that the 'universal' numbers $C_A$ defined above, that characterize the lack of self-averaging at $T_c$ in a random system, do differ for these two choices (Wiseman and Domany, 1998). In a sense these two choices to fix the concentration of the random alloy correspond to the canonical and semi-grand canonical ensemble of statistical mechanics. If we were to treat the disorder as 'annealed' rather than 'quenched' for annealed disorder, the average would simply be

$$\langle A\{S_i, c_i\} \rangle_T = \frac{1}{Z} \underset{\{S_i, c_i\}}{\text{Tr}} A\{S_i, c_i\} \exp(-\mathcal{H}\{S_i, c_i\}/k_B T), \qquad (5.30)$$

i.e. in the trace the two types of variables $\{S_i\}$, $\{c_i\}$ are now both included, and treated on an equal footing – so the local concentration on the lattice site also exhibits thermal fluctuations (e.g. due to interdiffusion of the species A, B in the crystal), unlike the quenched case. In the semi-grand canonical

ensemble of alloys, the chemical potential difference $\Delta\mu = \mu_A - \mu_B$ between the species is the independent thermodynamic variable, and then the concentration undergoes thermal fluctuations, while in the canonical ensemble $x$ is the independent thermodynamic variable and hence strictly non–fluctuating (thermal fluctuations then occur in the conjugate variable $\Delta\mu$, but this variable often is not even recorded in a simulation). These distinctions between the various thermodynamic ensembles naturally have analogs for the calculation of quenched averages, since one can consider quenched averaging as an averaging of the disorder variables ($\{c_i\}$ in our example) as a thermal averaging at a different (higher) temperature: for a completely random selection of lattice sites, we average at infinite temperature. We can introduce some correlations in the occupancy of lattice sites by defining

$$P\{c_i\} = \frac{1}{Z_0} \exp(-\mathcal{H}_c\{c_i\}/k_B T_0), \qquad (5.31)$$

where $\mathcal{H}_c$ is some model Hamiltonian describing the 'crystallographic' interaction between the species A, B, and one assumes that at the temperature $T_0$ ($\gg T$) the $\{c_i\}$ are still in full thermal equilibrium, before one quenches in the configurations of the $\{c_i\}$ thus generated by sudden cooling from $T_0$ to $T$, where the $\{c_i\}$ are forbidden to relax. Obviously, these considerations are motivated by the actual experimental procedures, but they also clarify that the different ensembles with which the averaging at $T_0$ is performed lead to different ensembles for carrying out quenched averages. In most cases one considers uncorrelated disorder, i.e. $1/T_0 \to 0$, but these considerations apply in this limit as well.

One important aspect about quenched averaging is that the distribution $P(A)$ generated in this way ($[\langle A\{S_i, c_i\}\rangle]_{av} = \int dA\, P(A)A$) typically is not symmetric around its average, mean value and most probable value may differ appreciably. Consider, for instance, the magnetization for the above model Hamiltonian at a temperature slightly above the average value of $T_c(L)$: those samples for which $T_c(L) > T$ due to the sample-to-sample fluctuation of $T_c(L)$ will have a large magnetization, while those samples where $T_c(L)$ deviates in the other direction will have a very small magnetization. This asymmetry of the distribution creates problems if one calculates quantities which have very small averages, e.g. spin correlations $[\langle S_i S_j\rangle_T]_{av}$ with large distances $\mathbf{r}_i - \mathbf{r}_j$ between the sites $i, j$.

An even more subtle effect may occur due to extremely rare fluctuations. Consider e.g. the case of simple dilution in the above model Hamiltonian, where $\mathcal{J}_{AB} = \mathcal{J}_{BB} = 0$, $\mathcal{J}_{AA} \equiv \mathcal{J}$. Then for $x < 1$ the critical temperature $T_c(x)$ will be clearly less than $T_c(1)$. However, the probability is non-zero (albeit extremely small) that somewhere in the system we find a large compact region free of dilution sites. This region will effectively order already at $T_c(1)$, in a still disordered environment. A mathematical consideration of this problem shows that there is a whole temperature region $T_c(x) < T < T_c(1)$ where very weak singularities are already present (known as 'Griffiths singularities'; Griffiths, 1969). One also expects that these singularities cause some anomalous tails in

dynamic correlation functions at long times, but due to problems of sampling such very small correlations accurately enough this problem is not yet so well understood.

Monte Carlo simulation of systems with quenched disorder is a difficult task; due to the need of carrying out the double averaging procedure over both thermal disorder and quenched disorder the demand for computer resources is huge and the judgement of the accuracy is subtle, particularly due to metastability and slow relaxation at low temperatures. Many problems are still incompletely understood. In the following, we mention two types of problems more explicitly, but only on the level of rather introductory comments. For extensive reviews of the state of the art in this field, we refer to Young (1998).

### 5.4.2 Parallel tempering: a general method to better equilibrate systems with complex energy landscapes

The standard method to equilibrate systems with quenched disorder at low temperatures relies on a slow cooling from high temperature to the temperature of interest. (The same is true for other systems with a broad spectrum of large relaxation times such as undercooled fluids near the glass transition to an amorphous solid.) A quite different approach has also been proposed to accelerate Monte Carlo simulations in systems with complex behavior. In this method, called 'parallel tempering' (Hukushima and Nemoto, 1996) or 'replica exchange' (Swendsen and Wang, 1986), multiple copies of the system, each at a different temperature $T_i$, are simulated simultaneously. In addition to the usual single site trial moves, occasionally an interchange of temperature between two systems at neighboring temperatures is attempted. The probability of such an exchange occurring is (as shown figuratively below)

$$T_1 \quad T_2 \quad T_3 \quad T_4 \quad T_5 \ldots$$

$$p(i \rightarrow j) = \min\left[1, e^{(E_i - E_j)(\beta_i - \beta_j)}\right], \tag{5.32}$$

where $\beta_i = 1/k_B T_i$. This approach had been proposed earlier, and independently, by Geyer (1991) in a computer science publication that is not often noticed by physicists. The effect is to 'feed' fluctuations that occur at higher temperatures into systems at lower temperatures. There should be overlap between the probability distributions of the systems at the two temperatures in order for such exchanges to be successful, and some care must thus be used in choosing the temperatures of all of the systems being simulated. The method is particularly useful for systems with multiple energy barriers, e.g. spin glasses, for which cluster methods are not efficient. An example of the successful application of this technique will be given in Section 5.4.5. Because the different replicas are simulated largely independently of each other, the method is well suited for parallel systems without a high speed connection between different processors.

Parallel tempering should not be confused with simulated tempering, an extended ensemble method that was proposed independently by Marinari and Parisi (1992) and Lyubartsev *et al.* (1992). In simulated tempering, a single system is simulated but the temperature is treated as a stochastic variable so that after a fixed number of 'ordinary' trial moves an attempt is made to change the temperature by a small amount. This process involves an additional function that is a priori unknown. Hence, it is usually necessary to perform a 'standard' simulation to estimate this function and then iterate the process to improve the estimate. Because of this complexity, simulated tempering has been used less than parallel tempering.

### 5.4.3 Random fields and random bonds

The presence of certain kinds of randomness leads to some of the most complex behavior in statistical physics and occurs in several different kinds of deceptively simple models (see Young, 1996). (In this section we shall not discuss the case of spin glasses at all since these will be treated separately.) If a simple Ising ferromagnet is subjected to a magnetic field which is randomly up or down, what happens to the phase transition? This quite straightforward question is surprising difficult to answer. Imry and Ma (1975) examined the question of whether or not the groundstate would be ordered by considering the competition between the surface energy that would be needed by producing a domain of overturned spins and the Zeeman energy that would be gained. They concluded that for lattice dimension $d \leq d_l = 2$ an ordered state would be unstable against the formation of domains. (For continuous spins, $d_l = 4$.) These, and other random field models, have been simulated extensively; but the long correlation times and the need to average over different realizations of the random field have produced data which have been interpreted in different ways, including the presence of first order transitions for at least a portion of the phase diagram and a new two–exponent hyperscaling relation. The breakdown of standard hyperscaling requires modifications of the finite size scaling approach. Despite the investment of substantial computing resources (note $10^4$ samples of random field configurations were used for averages) $L \times L \times L$ lattices with $L > 16$ were inaccessible due to excessively long relaxation times. Unlike 'pure' Ising systems, where no random fields are present, an accurate estimation of critical exponents for the random field Ising model does not yet seem to be possible. At this time there is still a pressing need for a dramatically improved algorithm to allow the unambiguous determination of the nature of the phase diagram.

For the case of random bond models in the absence of an applied field the situation is equally intriguing. Two separate kinds of problems have already been examined, although the descriptions are by no means complete. For $q$-state Potts models with large $q$ the transition is known to be first order. A somewhat surprising prediction was made by Hui and Berker (1989) that the presence of two different strength ferromagnetic bonds would change the order of the transition to second order. This behavior was indeed observed

by Chen *et al.* (1995) who used a 'multihit' Swendsen–Wang algorithm and histogram reweighting (see Chapter 7) to study the phase transition in the two–dimensional $q = 8$ Potts model with exactly 50% of weak bonds randomly spread throughout the lattice, a fraction for which the exact transition temperature is known. Their finite size analysis yielded critical exponents which were consistent with two-dimensional Ising values. Although there are now more refined predictions (Cardy and Jacobsen, 1997) that the exponents are not quite Ising–like, there is still no broad understanding of the effect of different kinds of randomness on first order transitions. If the transition is second order in the absence of any randomness there may again be several kinds of phenomena which result. If the randomly dispersed bonds are of zero strength, one can study the nature of the critical behavior, both for small dilution as well as when the percolation threshold is approached. Extensive Monte Carlo simulations of the bond impure two-dimensional Ising model have suggested that the critical behavior is modified by logarithmic corrections (Selke *et al.*, 1994). Random antiferromagnetic bonds can also lead to frustration, although this does not necessarily destroy the transition if the percentage of bonds is below a critical value.

### 5.4.4 Spin glasses and optimization by simulated annealing

Spin glasses are disordered magnetic systems, where the interactions are 'frustrated' such that no groundstate spin configuration can be found that is satisfactory for all the bonds (Binder and Young, 1986). Experimentally, such quenched disorder in the exchange constants is found in many strongly diluted magnets, e.g. a small percentage of (magnetic) Mn ions in a random Cu–Mn alloy interact with the Ruderman–Kittel indirect exchange which oscillates with distance as $\mathcal{J}_{ij} \propto \cos(k_F|\mathbf{r}_i - \mathbf{r}_j|)/|\mathbf{r}_i - \mathbf{r}_j|^3$, where the Fermi wavelength $2\pi/k_F$ is in general incommensurate with the lattice spacing. Since in such a dilute alloy the distances $|\mathbf{r}_i - \mathbf{r}_j|$ between the Mn ions are random, both ferro- and antiferromagnetic $\mathcal{J}_{ij}$ occur approximately with equal probability. Qualitatively, we may model such systems as Ising models with a Gaussian distribution $P(\mathcal{J}_{ij})$, see Eqn. (4.72), or by the even simpler choice of taking $\mathcal{J}_{ij} = \pm \mathcal{J}$ at random with equal probability as shown in Eqn. (4.73). A plaquette of four bonds on a square with three $+\mathcal{J}$ and one $-\mathcal{J}$ is enough to demonstrate the frustration effect: it is an easy exercise for the reader to show that such an isolated plaquette that is frustrated (i.e. sign $(\mathcal{J}_{ij}\mathcal{J}_{jk}\mathcal{J}_{kl}\mathcal{J}_{li}) = -1$) has an energy $-2\mathcal{J}$ and an eight-fold degenerate groundstate, while for an unfrustrated plaquette the energy is $-4\mathcal{J}$ and the degeneracy only two-fold. An example of frustration, as well as a schematic 'energy landscape' for a frustrated system, is shown in Fig. 5.8. Note that in reality phase space is multidimensional, not one-dimensional, and finding low lying minima as well as optimal paths over low lying saddle points is still quite a challenge for simulations. An approach for tackling this challenge can be based on 'multicanonical sampling' (Berg and Neuhaus, 1991, 1992), as will be described in Section 7.6.
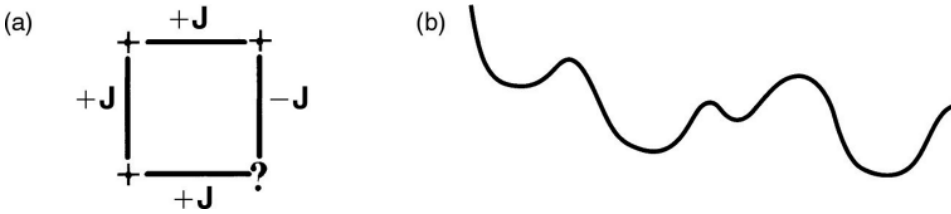
(a)

(b)



Fig. 5.8 (a) Frustrated plaquette in an Ising model with three $+\mathcal{J}$ and one $-\mathcal{J}$ bonds; (b) schematic view of an 'energy landscape' in a spin glass.

Spin glasses are viewed as archetypical examples of disordered solids in general (glasses, amorphous plastic materials, rubber, gels, etc.), and for several decades Monte Carlo simulations have been a part of this mainstream topic in condensed matter research. Thus we will provide a brief, tutorial introduction to this subject (more thorough discussions about spin glasses and other disordered materials can be found in Binder and Kob (2011)). The experimental hallmark of spin glasses is a cusp (or kink) in the zero field static susceptibility and while mean field theory for an infinite range model (Edwards and Anderson, 1975) shows such a behavior, the properties of more realistic spin glasses have been controversial for a long time. As has already been emphasized above, for systems with such quenched disorder, a double averaging is necessary, $[\langle \ldots \rangle_T]_{av}$, i.e. the thermal average has to be carried out first, and an average over the random bond configuration (according to the above probability $P(\mathcal{J}_{ij})$) afterwards. Analytic techniques yield only rather scarce results for this problem, and hence Monte Carlo simulations are most valuable.

However, Monte Carlo simulations of spin glasses are also very difficult to perform due to slow relaxation caused by the existence of many states with low lying energy. Thus, when one tries to estimate the susceptibility $\chi$ in the limit $H \to 0$, the symmetry $P(\mathcal{J}_{ij}) = P(-\mathcal{J}_{ij})$ implies that $[\langle S_i S_j \rangle_T]_{av} = \delta_{ij}$ and hence

$$\chi = \frac{1}{k_B T} \left( \sum_j [\langle S_i S_j \rangle_T - \langle S_i \rangle_T \langle S_j \rangle_T]_{av} \right) = \frac{1}{k_B T}(1 - q), \quad (5.33)$$

where

$$q = \left[ \langle S_i \rangle_T^2 \right]_{av},$$

i.e. the cusp would result from onset of a spin glass order parameter $q$ below the freezing temperature $T_f$. In the Monte Carlo simulation, the thermal averaging $\langle \cdots \rangle_T$ is replaced by time averaging, and hence (Binder, 1977)
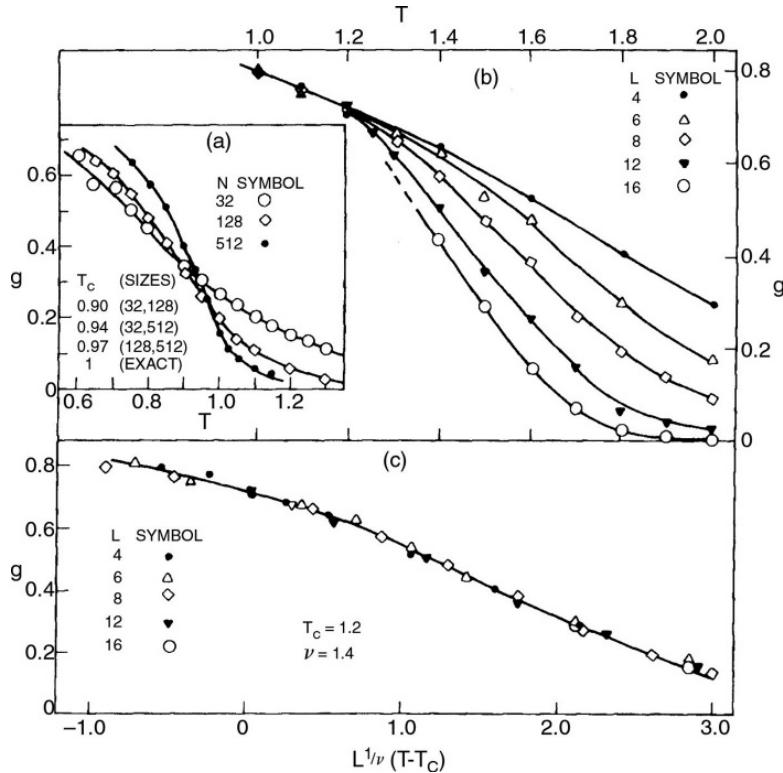
$$\chi = \frac{1}{k_B T}(1 - q(t)), \quad (5.34)$$

where

$$q(t) = \left[ \left( \frac{1}{t} \int_0^t S_i(t')\, dt' \right)^2 \right] = \left[ \frac{2}{t} \int_0^t \left( 1 - \frac{t'}{t} \right) \langle S_i(0) S_i(t') \rangle dt' \right].$$

Fig. 5.9 Plot of $g$ against $T$ for the three-dimensional SK $\pm\mathcal{J}$ Ising model. The lines are just guides to the eye. (a) Plot of cumulant intersections for the mean–field spin glass model; (b) temperature dependence of the cumulant; (c) scaling plot for the cumulant. From Bhatt and Young (1985).



This argument shows that an apparent (weakly time-dependent) spin glass order parameter $q(t)$ may arise if the spin autocorrelation function has not decayed during the observation time $t$. Thus Monte Carlo runs which are too short may show a cusp in $\chi$ as an observation-time effect, even if there is no transition at non-zero temperature in the static limit. This in fact is the explanation of 'cusps' found for $\chi$ in two-dimensional spin glasses (Binder and Schröder, 1976). It took great effort with dedicated machines (a special purpose processor for spin glass simulations was built by Ogielski (1985) at AT&T Bell Laboratories) or other advanced specialized computers, e.g. the 'distributed array processor' (DAP), to show that $T_f = 0$ for $d = 2$ but $T_f \approx 1.2\,\mathcal{J}$ for the $\pm\,\mathcal{J}$-model in $d = 3$. Again the cumulant intersection method, generalized to spin glasses (Bhatt and Young, 1985), turned out to be extremely useful: one considers the quantity

$$g_L(T) = \tfrac{1}{2}(3 \;-\; [\langle q^4 \rangle_T]_{\mathrm{av}} / [\langle q^2 \rangle_T]_{\mathrm{av}}^2),   \tag{5.35}$$

the $\langle q^k \rangle$ being the moments of the distribution of the spin glass parameter. The fact that the curves for $g_L(T)$ for various $L$ merge at $T_f$ is evidence for the existence of the transition (Fig. 5.9). No analytic method has yielded results competitive with Monte Carlo for this problem. Note, however, that the sizes that were used to produce Fig. 5.9 were necessarily quite small and the data

were limited in their statistical accuracy. However, good data with finer resolution show that there are still subtle finite size effects that cannot be discerned from the figure. Thus, the estimate for the critical temperature quoted in Fig. 5.9 is about 5% higher than the best estimates at the time of writing. Actually, estimating $T_f$ with high accuracy for this model is exceedingly difficult: Kawashima and Young (1996), using better averaging and larger lattices obtained $T_f/\mathcal{J} = 1.12(2)$, while Hatano and Gubernatis (1999) claimed that $T_f/\mathcal{J} \approx 1.3$; however, most researchers believe that the implementation of the 'multicanonical' Monte Carlo method (see Section 7.6) used by these latter authors leads to some systematic errors in their estimation of the spin glass order parameter distribution $P(q)$. In fact, a more recent study, by Ballesteros *et al.* (2000) yielded $T_f \approx \mathcal{J} 1.14$. Ballesteros *et al.* (2000) pointed out that a more reliable estimate of the critical temperature of spin glasses may be extracted from intersection points of the scaled finite size correlation length $\xi_L/L$ vs. temperature rather than from cumulant intersections (see Fig. 5.11 in Section 5.4.6 for an example of such a scaling analysis based on the correlation length). Actually, for spin glasses the extraction of a correlation length is subtle: as pointed out above, $[\langle S_i S_j\rangle]_{\text{av}} = \delta_{ij}$, so one must base the analysis on the spin glass correlation function $G_{SG}(\mathbf{r}) = [\langle S_i S_j\rangle^2]_{\text{av}}$, where $\mathbf{r} = |\mathbf{r}_i - \mathbf{r}_j|$ is the distance between the spins at lattice sites $i, j$. From the definition of a wave-vector-dependent spin glass susceptibility,

$$\chi_{SG}(\mathbf{k}) = N^{-1} \sum_{i,j} G_{SG}(\mathbf{r}) \exp(i\mathbf{k} \cdot \mathbf{r}),$$

$\xi_L$ may be defined via an expansion at small wave vectors $\mathbf{k}$, i.e. $\chi_{SG}(\mathbf{k}) = \chi_{SG}(0)/(1 + k^2\xi_L^2 + \cdots)$. In practice, only two wave vectors are needed, namely $\mathbf{k} = 0$ and $\mathbf{k} = \mathbf{k}_{\min} = (2\pi/L)(1, 0, 0)$, to obtain

$$\xi_L = \frac{1}{2\sin(\mathbf{k}_{\min}/2)} \left(\frac{\chi_{SG}(0)}{\chi_{SG}(\mathbf{k}_{\min})} - 1\right)^{1/2}.$$

At this point, we note the obvious advantage that simulations have over experiments: there is no experimental method known by which the spin glass correlation length could be measured for any real system. In fact, the question of whether real spin glasses exhibit a phase transition was settled (Binder and Young, 1986; Young, 1998) only when it was realized that at least the spin glass susceptibility $\chi_{SG}(0)$ could be estimated experimentally by analyzing the non–linear response of the magnetization to an external field.

Since spin glass model systems are very easily trapped in low-lying metastable states for $T < T_f$, it is very difficult to judge whether the system has been cooled down sufficiently slowly to reach true equilibrium. While techniques such as parallel tempering (Section 5.4.2) are clearly indispensable here, it is very desirable to have a stringent test for equilibration. Katzgraber *et al.* (2001) developed such a test for spin glasses with a symmetric Gaussian bond distribution $P(\mathcal{J}_{ij})$ (see Eqn. (4.72) with $\tilde{\mathcal{J}}_{ij} = 0$). Then, one can derive two expressions for the internal energy that are equivalent in thermal equilibrium,
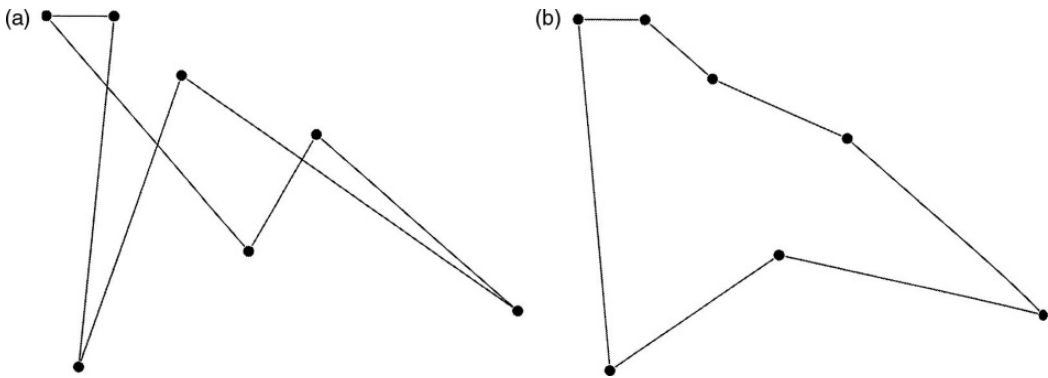
Fig. 5.10 Schematic view of the traveling salesman problem: (a) unoptimized route; (b) optimized route.

while during the equilibration process one expression approaches the equilibrium result from above and the other approaches it from below. Similarly difficult, of course, is the search for the groundstates of the spin glass: again 'simulated annealing', i.e. equilibration at high temperatures combined with very slow cooling, turns out to be relatively efficient. For a spin glass, the simple strategy given in Section 3.7 for finding a groundstate will *not* work.

Finding the groundstate energy of a spin glass is like solving an optimization problem, where the Hamiltonian is treated as a functional of the spin configuration, and one wishes to minimize this functional. Similar optimization problems occur in economics: e.g. in the 'traveling salesman problem' a salesman has to visit $n$ cities (with coordinates $\{x_k, y_k\}$) successively in one journey and wishes to travel such that the total distance $d = \sum_{\ell=1}^{n-1} d_\ell$, $\{d_\ell = \sqrt{(x_k - x'_k)^2 + (y_k - y'_k)^2}\}$ becomes a minimum: clearly the salesman then saves time, mileage, and gasoline costs, etc. A pictorial view of the 'traveling salesman problem' is shown for a small number of cities in Fig. 5.10. Now one can generalize this problem, treating this cost function like a Hamiltonian in statistical mechanics, and introduce 'temperature' into the problem, a term which originally was completely absent from the optimization literature. A Monte Carlo simulation is then used to modify the route in which the order of the visits of adjacent cities is reversed in order to produce a new trial state, and a Metropolis, or other, acceptance criterion is used. At high temperature the system is able to get out of 'local minima' and as the temperature is lowered it will hopefully settle to the bottom of the lowest minimum, i.e. the shortest route. This simulated annealing approach, introduced by Kirkpatrick *et al.* (1983) to solve global optimization problems, has developed into a valuable alternative to other schemes for solving optimization problems (Schneider and Kirkpatrick, 2006). It is thus a good example of how basic science may have unexpected economic 'spin-offs'. The invention of simulated annealing for spin glass simulations has had an impact on the general theory of optimization problems, e.g. in information science, economics, protein folding, etc., and has promoted the interaction between statistical physics and 'distant' fields. Applications of Monte Carlo simulation techniques and optimization

algorithms can in fact be combined in a very useful way. Indeed, a rich variety of methods for the study of groundstates and low-lying excited states for various model systems with randomly quenched disorder exist (Hartmann and Rieger, 2002). These techniques allow the study of problems ranging from polymers in random media to loop percolation of flux lines in disordered superconductors ('vortex glasses'), etc. Yet another interesting outcome of Monte Carlo simulations of spin glasses is research on neural networks (the simplest of which are Ising spin glasses with $J_{ij} \neq J_{ji}$) and information processing which have applications to cryptography and 'econophysics'. These topics are beyond the scope of this book, but introductions can be found in Nishimori (2001), Kinzel and Kanter (2003), and Mézard and Montanari (2009), as well as in the brief remarks in Chapter 13 of this text.

### 5.4.5 Ageing in spin glasses and related systems

Slow relaxation behavior in spin glasses has long been known to occur, and consequently increased attention has been given to the understanding of the non-equilibrium character of spin glasses. There is evidence, from both experiment and simulation, that random systems such as spin glasses never reach thermal equilibrium under conditions of practical interest, i.e. for realizable time scales. Then, so-called 'ageing' effects appear, e.g. for which a correlation function $\langle A(s)B(t'+s) \rangle$ depends not only upon the difference in time $t'$ between the two times but upon $s$ and $t = t' + s$ separately. Ageing phenomena and the development of a quasi-fluctuation-dissipation theorem (because of violations of the fluctuation-dissipation relation) have become a topic of substantial study, much of it by computer simulation (Crisanti and Ritort, 2003) which has guided the initial steps of the theoretical description. If one perturbs the system at time $t = 0$ and waits a time $s$ before making measurements, one can define quantities like the time-dependent susceptibility

$$X(t, s) = X_{st}(t - s) + X_{ag}(t, s), \qquad (5.36)$$

where the first term is the stationary part that asymptotically decays to a finite value, and the second term is the ageing term that obeys a scaling relation

$$\chi_{ag}(t, s) = \hat{\chi}\left(\frac{t}{s^x}\right). \qquad (5.37)$$

In many solvable models $x = 1$, but spin glass models suggest $x < 1$. (However, experiments report values quite close to $x = 1$.) These studies provide a glimpse of the often poorly understood behavior of non-equilibrium systems that will be discussed in more detail in Chapter 10.

### 5.4.6 Vector spin glasses: developments and surprises

Until rather recently the 'conventional wisdom' was that there was a spin glass transition in three-dimensional Ising models but not in Heisenberg models, i.e. the transition was believed to occur only at $T_{SG} = 0$. Using extensive Monte Carlo simulations on the Heisenberg spin glass model with a Gaussian

Fig. 5.11 Finite size behavior of the Gaussian Heisenberg spin glass in three dimensions. The inset shows a finite size scaling plot using $k_B T_{SG}/\mathcal{J} = 0.16$ and $\nu = 1.1$. After Lee and Young (2003).
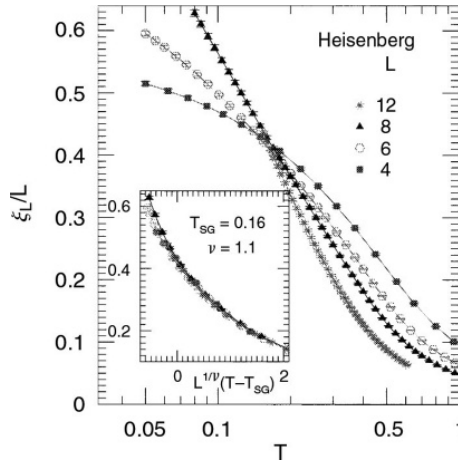


distribution of nearest neighbor bonds, Hukushima and Kawamura (2000) produced evidence for a chiral ordering transition at finite temperature. The finite size behavior of the reduced fourth order cumulant for the chirality showed a crossing at $k_B T/\mathcal{J} \sim 0.15$, but the lack of a similar crossing for a spin glass order parameter was considered to be evidence that there was no finite temperature transition that involved the spin degrees of freedom. By analyzing a different quantity, however, Lee and Young (2003) came to the (then) surprising conclusion that both spin and chiral degrees of freedom ordered at the same, non-zero temperature. They began by introducing 'parallel tempering' (see Section 5.4.2) to reach low temperatures at which equilibration would be otherwise very difficult. In addition, they developed new criteria to check that thermal equilibration had actually been achieved and calculated the wave vector dependent spin glass susceptibility in order to extract the finite lattice spin glass correlation length $\xi_L$. Then, using the finite size scaling form for this quantity, i.e.

$$\frac{\xi_L}{L} = \tilde{X}[L^{1/\nu}(T - T_{SG})], \tag{5.38}$$

they showed that curves for multiple sizes crossed at a single temperature (see Fig. 5.11) at which $T = T_{SG}$. The same procedure for the chiral correlation length yielded a transition at a temperature that was, within error bars, identical to that for the spin degrees of freedom. Thus, with the systematic implementation of new algorithms, substantial CPU time, and thoughtful analysis, they were able to discover an unexpected result. (This lesson can surely be applied to other problems in statistical physics.)

## 5.5 MODELS WITH MIXED DEGREES OF FREEDOM: Si/Ge ALLOYS, A CASE STUDY

There are many important models for which both discrete and continuous degrees of freedom must be incorporated. One example is an impure

Heisenberg model for which Ising degrees of freedom specify whether or not a site is occupied by a magnetic ion and continuous variables describe the behavior of the magnetic spins at the sites which are occupied. A Monte Carlo study must then include possible changes in both variables. A more complex situation arises when all states of the discrete variable are interesting and the potential associated with the continuous variable is complicated. A simple example is Si/Ge alloys. These systems are examples of semiconductor alloys which play an extremely important role in technological development. For purposes of industrial processing we need to know just what the phase diagram looks like, and more realistic models than simple lattice alloy models are desirable. These systems may be modeled by an Ising degree of freedom, e.g. $S_i = +1$ if the site is occupied by Si and $S_i = -1$ if a Ge is present, and $S_i = 0$ corresponds to a vacancy at a site. The second, continuous variable describes the movement of the nodes from a perfect lattice structure to model the disorder due to the atomic displacements of a crystal that is compressible rather than rigid. Elastic interactions are included so both the local and global energies change as the system distorts. These systems are known to have strong covalent bonding so the interactions between atoms are also strongly directional in character. The empirical potentials which seem to describe the behavior of these systems effectively thus include both two-body and three-body terms. In order to limit the effort involved in calculating the energies of states, a cutoff was implemented beyond which the interaction was set to zero. This model was studied by Dünweg and Landau (1993) and Laradji *et al.* (1995) using a 'semi-grand canonical ensemble' in which the total number of atoms was fixed but the relative numbers of Si and Ge atoms could change. Monte Carlo 'moves' allowed an atom to be displaced slightly or to change its species, i.e. Si → Ge or Ge → Si. (The chemical potential $\mu$ represented the difference between the chemical potentials for the two different species; the chemical potential for vacancies was made so large that no vacancies appeared during the course of the simulation.) The simulation was carried out at constant pressure by allowing the volume to change and accepting or rejecting the new state with an effective Hamiltonian which included the translational entropy, i.e.

$$\Delta \mathcal{H}_{\mathrm{eff}} = \Delta \mathcal{H} - N k_{\mathrm{B}} T \ln \frac{\Lambda'_x \Lambda'_y \Lambda'_z}{\Lambda_x \Lambda_y \Lambda_z}, \tag{5.39}$$

where $\Lambda$ and $\Lambda'$ represent the dimensions of the simulation box and of the trial box, respectively.

The data were analyzed using the methods which have been discussed for use in lattice models and showed, somewhat surprisingly, that the transition was mean-field in nature. The analysis was not altogether trivial in that the critical point was located using a two-dimensional search in $(\mu - T)$ space (using histograms which will be described in Chapter 7). The behavior of the fourth order cumulant of the order parameter and the finite size scaling of the 'susceptibility' are shown in Fig. 5.12; both properties demonstrate clearly that the critical point is mean-field in nature. The first study, carried out with the Keating valence field potential yielded a somewhat surprising and unphysical
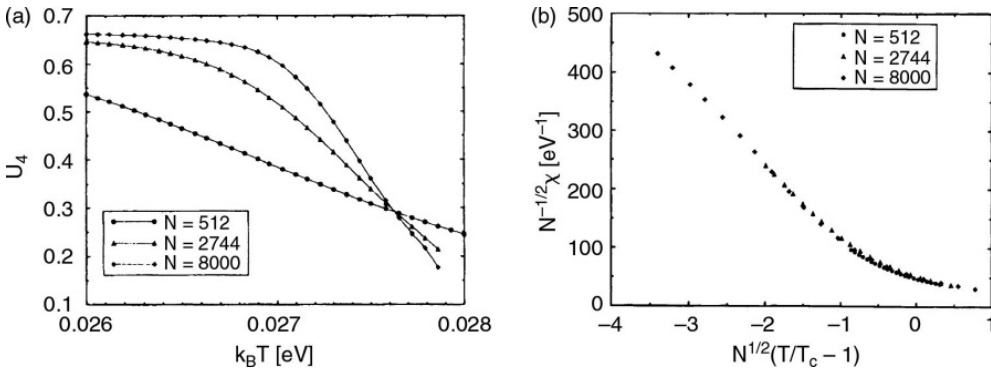
Fig. 5.12 Elastic Ising Si/Ge model data obtained using a Keating potential: (a) fourth order cumulant crossing; (b) finite size scaling of the 'susceptibility' using mean-field exponents. After Dünweg and Landau (1993).

result in that the lattice constant shrank continuously as the temperature was raised. When the calculations were repeated with the Stillinger–Weber potential, this effect disappeared. This showed the importance of not relying solely on fitting low temperature properties in designing phenomenological potentials for the description of real alloys.

## 5.6 METHODS FOR SYSTEMS WITH LONG RANGE INTERACTIONS

As computer speeds have increased researchers have attempted to simulate more realistic models, and, in many cases, this means including long range interactions. This is a special challenge for lattice systems of the type that we have been discussing since sampling methods are typically so extremely efficient and fast that the treatment of long range interactions must also be very efficient if it is not to slow down the simulation severely. Luijten and Blöte (1995) introduced an artful cluster algorithm for the Ising model in which the number of operations per spin-flip was reduced from $\mathcal{O}(N^2)$ to $\mathcal{O}(N \log N)$ by reformulating the cluster construction process. More recently Sasaki and Matsubara (2008) proposed an even more efficient and general method that eliminates interactions stochastically and replaces the remaining interactions by a pseudo-interaction so as to produce an $\mathcal{O}(N)$ algorithm.

In considering a system with interactions $V_{ij}$ between spins that are at positions $r_i$ and $\mathbf{r_j}$, the first step is to introduce the set of pairs $\{C_{\mathrm{pair}}(r)\}$ for all spins in the system separated by a distance $r = |\mathbf{r}_i - \mathbf{r}_j|$. The potential between pairs of spins $(\mathbf{S_i}, \mathbf{S_j})$ will be switched to a pseudo-potential with probability $P_{ij}$ or switched off (i.e. set equal to zero) with probability $1 - P_{ij}$ where $P_{ij}$ is determined by the nature of the long range interaction. In most cases the probability of switching off the potential for a pair in $\{C_{\mathrm{pair}}(r)\}$ has a maximum value $p_{\mathrm{max}}(r)$. Using $p_{\mathrm{max}}$ one then identifies 'candidates' for switching

and sets each equal to the pseudo–potential interaction with probability $[1 - P_{ij}(S_i, S_j)]/p_{max}(r)$ or to 0 otherwise.

The important 'trick' in the algorithm is to avoid treating every pair in turn. If we denote the potential for a pair in $\{C_{pair}(r)\}$ by $V^{(k)}$, the probability that $V^{(n)}$ is chosen as a candidate after $(n-1)$ failures is given $g(p_{max}(r), n)$, where

$$g(p, n) = (1 - p)^{-1} \qquad (n \geq 1). \tag{5.40}$$

A random integer $n$ that obeys $g(p, n)$ can be easily generated as

$$n = \left[ \frac{\log(r)}{\log(1 - p)} \right]. \tag{5.41}$$

---

**The stochastic cutoff potential switching scheme for long range interactions**

1. Set $n_s = 0$, where $n_s$ is the number of potentials that have already been switched
2. Generate an integer $n$ from the distribution $g(p_{max}(r), n)$ using Eqn. (5.41). If $n = 1$, go to step (4). Otherwise, go to the next step
3. Switch the $(n-1)$ potentials ($V^{(n_s+1)}, V^{(n_s+2)}, \dots, V^{(n_s+n-1)}$) to 0.
4. Switch ($V^{(n_s+n)}$) to ($\overline{V}^{(n_s+n)}$) with probability $[1 - P^{(n_s+n)}(S_i, S_j)]/p_{max}(r)$. Otherwise, switch it to 0
5. Finish the potential switching procedure if ($n_s + n$) is greater than (or equal to) the number of elements of $\{C_{pair}(r)\}$. Otherwise, replace $n_s$ with ($n_s + n$) and go to step (2)
6. Continue until switching of all the potentials in $\{C_{pair}(r)\}$ is completed

---

Sasaki and Matsubara (2008) applied this method to $L \times L$ Heisenberg square lattices with nearest neighbor, isotropic exchange, and dipolar interactions between all spins. They verified that the results using the stochastic cutoff (SCO) method were the same as with the full, brute force method but, as shown in Fig. 5.13, the CPU time needed increased in proportion to the number of spins $N$. Sasaki (2009) reformulated the algorithm to derive new expressions for the internal energy and heat capacity and make replica exchange Monte Carlo (see Section 5.4.2) more efficient for systems with long range couplings.

A similar strategy was used by Fukui and Todo (2009) to produce an efficient method that adopted a different pseudo–interaction and a different way of switching interactions. We should also mention that a nice Fourier Monte Carlo method was introduced (Tröster, 2007) for investigating critical behavior in lattice systems with long range forces. This approach has proven to be valuable for elastic $\varphi^4$ and Ising models (Tröster, 2008a, 2008b) and crystalline membranes (Tröster, 2013) but has not yet found general utility.

Fig. 5.13 Average computational time per MC step $t_{av}$ for a $L \times L$ Heisenberg model square lattices with both nearest neighbor exchange coupling and dipolar interactions between all spins as a function of $N = L^2$ for the SCO method (solid squares) and the brute force method (open circles). From Sasaki and Matsubara (2008).
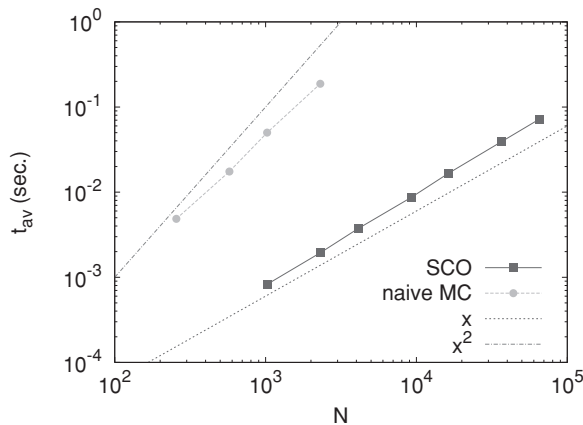


## 5.7 PARALLEL TEMPERING, SIMULATED TEMPERING, AND RELATED METHODS: ACCURACY CONSIDERATIONS

The method of 'parallel tempering' (PT) was already briefly introduced (Section 5.4.2) within the context of efficient simulation of systems with complex free energy landscapes (such as spin glasses, or models for the glass transition of fluids to amorphous solids, etc.). As was mentioned there, $n$ 'replicas' of the system are simulated in parallel at temperatures $\{T_i, i = 1, \ldots, n\}$ such that $T_1$ is the lowest temperature of interest, typically chosen below the transition to the (spin) glass phase, while the highest temperature $T_n$ is in the high temperature, disordered phase. In addition to the ordinary Monte Carlo trial moves that are carried out at fixed temperature, additional moves are considered for which a replica at temperature $T_i$ attempts an exchange with a 'neighboring' replica (i.e. at temperature $T_{i+1}$ or $T_{i-1}$). (In the simplest case, the inverse temperatures $\beta_i = (k_B T_i)^{-1}$ are equidistant, but other choices are conceivable.) Of course, very natural immediate questions are: 'How many temperatures $n$ should one choose for a particular case?'; 'Is it better to do the 'replica exchanges' (recall that 'parallel tempering' is also called 'replica exchange Monte Carlo') rather frequently or more seldom?'; and 'How does the error for a given investment of computer resources compare with the error of independent simulations where no exchanges take place?'

The careful reader will have noted that these questions have not been considered in Section 5.4.2; indeed, for systems with complex free energy landscapes one cannot give generally valid answers to any of these questions. However, it turns out that parallel tempering is also useful for somewhat simpler systems where the free energy landscape has only two minima separated by a high free energy barrier and the system is easily trapped in the metastable minimum at low temperatures. A much studied example for this class of problems is the folding/unfolding transition of short proteins, where often the analogous technique of 'replica exchange Molecular Dynamics' (REMD) is

used (e.g. Nadler and Hansmann, 2007a, 2007b, 2008; Rosta and Hummer, 2009). Although in the latter case positions (and momenta) of atoms evolve according to Newton's equations of motion (see Section 12.2), each replica is coupled to a 'thermostat' (at temperature $T_i$ for the $i$th replica), so the degrees of freedom are distributed according to the canonical ensemble. The crucial temperature exchange step ($T_i \rightarrow T_{i+1}$ or $T_{i-1}$) is attempted using the standard Metropolis acceptance probability, Eqn. (5.31a), so REMD has some character of a Monte Carlo method. Since we shall return to the problem of protein folding in a later chapter (Section 14.2), we defer a discussion of whether REMC or REMD methods are advantageous for such problems to this later chapter. But we emphasize here that there are many other cases of 'two-state models' with transitions between the states separated by high free energy barriers in physics: for example, in Section 4.2.3 we have discussed the thermally driven phase transition of the $q$-state Potts model (Eqn. (2.43)) with large $q$. Another example would be the crystallization transition of short polymers in poor solvents that can be modeled by the bond fluctuation model (Section 4.7) with attractive monomer–monomer interaction (Rampf *et al.*, 2005). It turns out that parallel tempering applications to such problems provide definitive answers to the questions posed above only in the limit of very long runs where the running time greatly exceeds the 'round trip time' needed for a replica to 'diffuse' back and forth over the full range of temperatures from $T_1$ to $T_n$. In order to achieve this, replica exchange needs to allow fast, but not too fast, relaxation of the energy of a replica to 'local equilibrium' in between subsequent exchange attempts. Of course, the order parameter of the transition between the two competing states (e.g. the fraction of a protein that is in the folded state) may relax much slower than the energy, and at very long times the dynamics would then be a single slow, exponential relaxation process characterized by the order parameter relaxation time.

The motions of the replicas through the temperature space $\{T_i, i = 1, \ldots, n\}$ can be described either in terms of master equations (Nadler and Hansmann, 2007a, 2007b, 2008) or with a treatment based on transition rates similar to descriptions of chemical kinetics (Rosta and Hummer, 2009). The latter treatment yields a formula which gives insight into the efficiency of this parallel tempering (PT) method; namely one compares the variance $\langle (\delta A)^2 \rangle_{T_k}$ of an observable $A$ at a temperature $T_k$ (as observed at a standard simulation) with the variance obtained from a PT study,

$$\eta_k = \frac{\langle (\delta A)^2 \rangle_{T_k}}{n \langle (\delta A)^2 \rangle_{T_k}^{\mathrm{PT}}} = \frac{1}{n} \sum_{i=1}^{n} \frac{\tau_k^+ + \tau_k^-}{\tau_i^+ + \tau_i^-}, \tag{5.42}$$

where $\tau_i^+$, $\tau_i^-$ are the lifetimes of the system in its two long-lived states (corresponding to the two competing minima of the free energy landscape), when the system is at temperature $T_i$. It is assumed that the same computational effort is invested for the runs at $\{T_i\}$ with and without replica exchange, and the actual computational overhead for the exchange moves is neglected. If $\eta_k > 1$ it is more efficient to carry out a PT simulation rather than doing a

standard simulation only at $T_k$ but $n$ times as long. Of course, one can enhance the accuracy at $T_k$ by including the neighboring temperatures into the computation of averages via histogram reweighting methods (see Chapter 7); it may also be of physical interest to obtain reliable averages not just for a single temperature $T_k$, but for the full range $\{T_i, i = 1, \ldots, n\}$. However, since the distributions of the internal energy at neighboring temperatures $\{T_i, T_{i\pm1}\}$ must strongly overlap to ensure a large enough acceptance for the exchange moves, it is clear that the method is useful in practice only for relatively small systems (otherwise $n$ has to be very large, and the computational effort gets out of hand). It is also clear that optimizing the number of replicas and temperature range $T_n - T_1$ is a subtle issue that may require careful tests; but for many systems, protein folding being just one example, this approach may be advantageous.

We mentioned earlier that a somewhat similar technique exists, under the name of 'simulated tempering' (ST), which also works with a system that can be in a set of discrete temperatures $\{T_i, i = 1, \ldots, n\}$. However, while in parallel tempering the sampling effort at all temperatures is the same by construction, in simulated tempering the idea is that a single system diffuses through the considered discrete temperature space. The times that the system spends at the different temperatures can be very different so, in a sense, the temperature of the system is like a standard dynamical variable.

In simulated tempering (ST) the transition probability for the temperature is given by the following acceptance probability

$$P_{\mathrm{acc}}(T_i \rightarrow T_f) = \mathrm{Min}\left\{1, \exp\left(\frac{E}{k_{\mathrm{B}} T_i} - \frac{E}{k_{\mathrm{B}} T_f} + f_f - f_i\right)\right\}, \quad (5.43)$$

where $E$ is the potential energy of the system, and $\{f_i\}$ are constants that determine the fraction $Q_i$ of time spent at $T_i$ in long runs,

$$Q_i = \exp(f_i)Z_i \Big/ \sum_{i=1}^{n} \exp(f_i)Z_i, \quad (5.44)$$

$Z_i$ being the partition function of the system at temperature $T_i$. The set $\{f_i\}$ can be optimized to achieve a targeted distribution of the $Q_i$; if $Q_i = 1/n$, the method becomes identical to parallel tempering, of course. In Eqn. (5.43) it was assumed that the generation probabilities for the changes $T_i \rightarrow T_f$ and $T_f \rightarrow T_i$ are identical. In a similar manner as for parallel tempering, one can derive an expression for the variance (Rosta and Hummer, 2010)

$$\eta = \frac{\langle(\delta A)^2\rangle_{T_k}}{\langle(\delta A)^2\rangle_{T_k}^{\mathrm{ST}}} = \sum_{i=1}^{n} Q_i \frac{\tau_k^+ + \tau_k^-}{\tau_i^+ + \tau_i^-}, \quad (5.45)$$

again assuming very long runs for a problem with two minima, as done above. One sees that for $Q_i = 1/n$ the PT result, Eqn. (5.42), indeed is recovered. Again the quality of the results can be improved by combining the technique with histogram reweighting.

Rosta and Hummer (2010) have also presented extensive tests of their theoretical arguments on PT and ST Monte Carlo simulations by numerical

studies of a $12 \times 12$ Ising ferromagnet. Of course, such an application is still far from systems of practical interest, and investigations of the theoretical aspects of PT and ST methods are still needed for more complicated and more realistic systems in the future.

## 5.8 SAMPLING THE FREE ENERGY AND ENTROPY

### 5.8.1 Thermodynamic integration

There are circumstances in which knowledge of the free energy itself, and not just its derivatives, is important. For example, at a strongly first order transition the bulk properties of a system will generally show pronounced hysteresis which makes a precise determination of the equilibrium location of the transition problematic. This problem can be largely avoided, however, by the determination and subsequent comparison of the free energies of different phases. The expressions given in Chapter 2 which provide a thermodynamic definition of the free energy $F$, can be used rather straightforwardly to actually provide numerical estimates for $F$. Since the internal energy $U$ can be measured directly in a Monte Carlo simulation and the entropy can be obtained by integrating the specific heat $C$, i.e.

$$S(T) = \int_0^T \frac{C(T')}{T'} \, dT'. \tag{5.46}$$

Of course, Eqn. (5.46) only makes sense for Ising-type systems, for which $C(T \rightarrow 0) \rightarrow 0$, but not for 'classical' systems for which $C(T \rightarrow 0) \rightarrow$ const. and the entropy $S(T \rightarrow 0) \rightarrow -\infty$. In some cases the free energy in a low temperature state can be accurately estimated and used to determine the free energy at finite temperature. (For example, in an Ising model it will be given by the internal energy at $T = 0$.) Alternatively, the free energy may be estimated in the high temperature, disordered state by integrating the internal energy, i.e.

$$\frac{F(T)}{k_B T} = -\frac{S(\infty, \; H)}{k_B} + \int_0^{1/k_B T} U d(1/k_B T). \tag{5.47}$$

The intersection of these two free energy branches (see Fig. 5.14a) determines the location of the transition. In some cases, however, the transition is encountered not by varying the temperature but rather by varying an applied field or chemical potential. In this case the appropriate thermodynamic integration becomes a two-step process as shown in Fig. 5.14b. Two different paths of constant field on opposite sides of the transition line are followed up to the desired temperature $T$ and the free energies are computed. The temperature
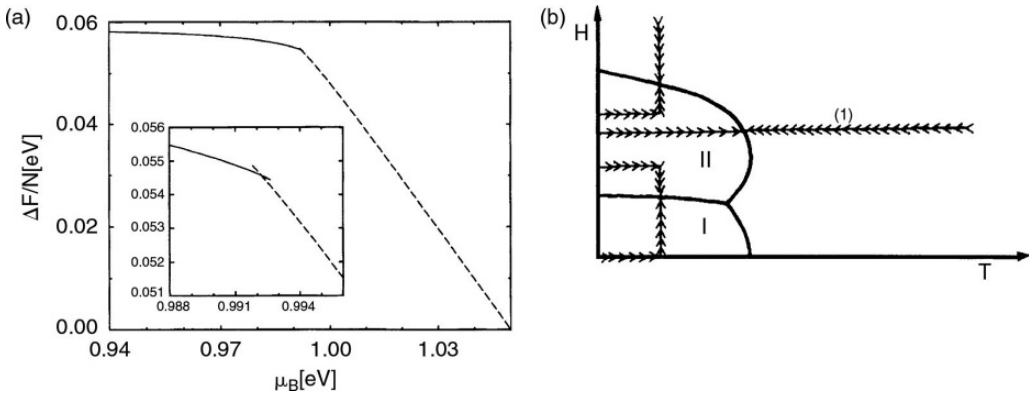
Fig. 5.14 (a) Comparison of free energies obtained with the chemical potential swept in opposite directions for the model of Si/Ge in the previous section. (b) Schematic view of paths for thermodynamic integration. In this figure there are three first order phase boundaries separating a high temperature disordered phase, and two low temperature ordered phases.

is then fixed and the field is then swept across the transition so that

$$F(H) = F(H_1, T) + \int_{H_1}^{H} M \, dH', \tag{5.48a}$$

$$F(H) = F(H_2, T) + \int_{H_2}^{H} M \, dH', \tag{5.48b}$$

and again the point of intersection locates the transition. The accuracy of this method is limited by the errors of the data points which are used for the integration and by residual finite size effects. (In addition to reducing the usual finite size effect, one must make the system large enough that there are no excursions to the other phase during a simulation run. The actual size that is needed depends on the magnitude of the discontinuities which occur at the transition.) Since the fluctuations are generally small near a first order transition, quite accurate data for large systems can be generated without too much difficulty, so the transition can be located quite accurately.

Thermodynamic integration can also be used for off-lattice models, e.g. for the Si/Ge model considered in Section 5.5. In addition, thermodynamic integration may be very useful in more complicated situations in which surface and interface phenomena play important roles. This topic will be considered in some detail in Section 6.8.

### 5.8.2 Groundstate free energy determination

For discrete spins the groundstate free energy is given simply by the internal energy. For systems with continuous variables, however, the groundstate entropy of classical systems is $-\infty$ and the determination of the entropy at low temperatures is non-trivial. One way to accomplish this is to divide the

Hamiltonian into two parts, one for which the groundstate free energy can be calculated theoretically, and the second part is a perturbation which is slowly turned on. The free energy change can be determined by integration over the prefactor describing the magnitude of the perturbation. One specific application of this approach is the method used by Frenkel and Ladd (1984) in which an Einstein crystal (whose free energy may be calculated exactly) is taken as the unperturbed system with the interparticle interactions slowly turned on to produce a harmonic solid. Integration as a function of the added interaction produces the desired estimate for the free energy. Dünweg and Landau (1993) introduced an alternative method which relied on the Monte Carlo sampling of the ratio of the partition functions for the two different phases using a form of umbrella sampling. This worked quite well for the Keating potential but is not necessarily effective for all potentials. When estimating the free energy of crystals with one of the above methods with the aim of distinguishing small free energy differences between different crystal structures, it is important to pay attention to small, but noticeable, finite size effects (see Polson *et al.*, 2000, and de Miguel *et al.*, 2007, for numerical evidence and discussion of this problem). Schilling and Schmid (2009) extended the Frenkel–Ladd method to disordered systems (e.g. fluids or glasses). They first produce a reference system using an equilibrated configuration of the system with particle–particle interactions 'turned off' and every particle fixed in its position by a harmonic potential. Then, an integration path is constructed for which the harmonic potential is gradually switched off and the interactions are gradually switched on until the desired Hamiltonian is achieved.

Finally, we remark that the search for the groundstate of arbitrary Hamiltonians can also be viewed as an optimization problem in which the energy of the system must reach a minimum (see Section 3.7). In such optimization treatments a 'cost function' is 'optimized', or, equivalently, the energy or free energy is minimized using, for example, 'simulated annealing' (see Section 5.4.4), 'genetic algorithms' (see Tipton and Henning, 2013, for a recent example and references), or Wang–Landau sampling (see Section 7.8).

### 5.8.3 Estimation of intensive variables: the chemical potential

In most of the methods that we have already discussed the intensive variable, e.g. magnetic field or chemical potential, was held fixed and the conjugate extensive variable, e.g. the magnetization or density, was measured. The inverse procedure, although more difficult, can also be carried out (Alexandrowicz, 1975; Meirovitch and Alexandrowicz, 1977). In the following we shall work in the language of a lattice gas model with nearest neighbor bond energy $-\varepsilon$, although the procedure for an Ising model would be completely equivalent. As previously seen in the discussion of the $N$-fold way, an occupied site would have five different possible 'local states' $\alpha$ depending on the number of nearest neighbor sites which were also occupied and would have energy $E_\alpha$. We then define a set of five conjugate states by removing the 'central' atom. This means that $E_{\alpha'} = 0$. If the probabilities of occurrence of each state are

$P(\alpha)$ and $P(\alpha')$, detailed balance requires that

$$\frac{P(\alpha)}{P(\alpha')} = \exp[(-E_\alpha + \mu)/k_{\mathrm{B}}T], \qquad (5.49)$$

so that

$$\frac{\mu}{k_{\mathrm{B}}T} = \ln\left(\frac{P(\alpha)}{P(\alpha')}\right) + \frac{E_\alpha}{k_{\mathrm{B}}T}. \qquad (5.50)$$

By averaging over all five different local states rather good statistical precision can be obtained for the estimate of the chemical potential. As we shall see in Chapter 6 there are specialized 'particle insertion' techniques which can be used to estimate the chemical potential when the lattice restriction is removed.

### 5.8.4 Lee–Kosterlitz method

The correct identification of the order of a transition can become particularly tricky if the transition is actually weakly first order. Lee and Kosterlitz (1990) proposed a very simple scheme which can be remarkably effective, even for quite small systems. A long simulation run is made at some value of the extensive 'field', e.g. temperature, which is quite near to the phase transition and a histogram of the order parameter values is constructed. If there are two peaks in the distribution, the distribution is reweighted to a different field value (see Chapter 7 for a detailed description of reweighting) until the two peaks are the same height, and the difference between the maxima and the minimum between the two peaks is used to estimate the free energy barrier $\Delta F$

$$\Delta F = \ln\frac{P_L(E_1)}{P_L(E_2)}, \qquad (5.51)$$

where $P_L(E_1)$ and $P_L(E_2)$ are the probabilities at the maximum and minimum values respectively. This procedure is repeated for different lattice sizes and if $\Delta F$ diverges with increasing size, the transition is first order in the thermo-dynamic limit. Otherwise, the transition is second order. This procedure was quite effective for small $q = 5$ Potts models even though a finite size scaling analysis for systems as large as $L = 240$ suggested that the transition was (incorrectly) second order.

### 5.8.5 Free energy from finite size dependence at $T_c$

A somewhat specialized but novel approach to the calculation of free energies at a critical point was proposed by Mon (1985). He considered the finite size variation of the free energy at the critical point for an $L^d$ system with periodic boundary conditions for which it is expected that

$$f_{\mathrm{sing}} \approx U_{\mathrm{o}}L^{-d}, \qquad (5.52)$$

where $U_{\mathrm{o}}$ is a scaling amplitude. The system is then decomposed into $2^d$ systems each of size $(L/2)^d$ and the ratio of the partition functions of the two

systems is given by

$$\frac{Z_{L/2}}{Z_L} = \frac{\operatorname{Tr} \exp(-\beta H_{L/2})}{\operatorname{Tr} \exp(-\beta H_L)} = \langle \exp[-\beta(H_{L/2} - H_L)] \rangle, \qquad (5.53)$$

where $H_L$ represents the Hamiltonian for the original system and $H_{L/2}$ is the Hamiltonian for the divided system. From Eqn. (5.53) we can see that the free energy difference between the two lattices is

$$f_L - f_{L/2} = \frac{\ln \langle \exp[-\beta(H_{L/2} - H_L)] \rangle}{L^d} \qquad (5.54)$$

and this relation, together with Eqn. (5.52) can be used to determine the singular part of the free energy. The estimation of the free energy difference in Eqn. (5.54) may not be easy to do directly but may be calculated using 'umbrella sampling', a method which will be described in the first part of Chapter 7.

## 5.9 MISCELLANEOUS TOPICS

### 5.9.1 Inhomogeneous systems: surfaces, interfaces, etc.

If a system contains surfaces or interfaces, its properties become position dependent. One particular strength of Monte Carlo simulation methods is that such effects can be studied in full detail and under perfectly well controlled conditions. For instance, let us stick to the example of the Ising ferromagnet that undergoes a phase transition at some critical temperature $T_{cb}$ in the bulk, characterized by the power laws already discussed in Chapter 2, e.g. the bulk magnetization $m_b = \hat{B}(1 - T/T_{cb})^\beta$, the bulk susceptibility $\chi_b = \hat{\Gamma}_\pm |1 - T/T_{cb}|^{-\gamma}$, etc. We now may ask (Binder, 1983) how this behavior gets modified when we consider the local counterparts of these quantities right in the surface plane ($m_1$, $\chi_1 = (\partial m_1/\partial H)_T$) or in the $n$th layer away from the free surface ($m_n$, $\chi_n$). Under which conditions does the surface order at a temperature $T_{cs}$ higher than the bulk, i.e. ($m_1 \propto (1 - T/T_{cs})^{\beta_{2d}}$ with $T_{cs} > T_{cb}$ and $\beta_{2d}$ is the two–dimensional Ising exponent)? If the surface layer orders at the same critical temperature as the bulk does, what are the associated exponents? ($m_1 \propto (1 - T/T_{cb})^{\beta_1}$, $\chi_1 \propto (1 - T/T_{cb})^{-\gamma_1}$). Actually, the surface involves many more exponents than the bulk does, since one can also consider the response to a local field $H_1$ ($\chi_{11} = (\partial m_1/\partial H_1)_T \propto (1 - T/T_c)^{-\gamma_{11}}$) and the critical behavior of surface excess quantities: the surface excess magnetization $m_s$ is defined in terms of the profile $m_n$ as $m_s = \sum_{n=1}^{\infty} (m_b - m_n)$, etc. In the simulation, all such questions can be addressed at once for well-defined models, control parameters (including local fields $H_n$ in arbitrary layers indexed by $n$, suitable changes $\Delta \mathcal{J} = \mathcal{J}_s - \mathcal{J}$ of the exchange coupling in the surface plane, etc.) can be varied at will, etc. Moreover, one can choose an absolutely ideal, perfect surface (no adsorbed 'dirt', no surface roughness, no dislocations, no grain boundaries, no surface steps, and so on). In all these respects, simulations have a huge advantage over experiments, and hence the testing of corresponding theory has proceeded, for the most part, by simulation methods. As Nobel

laureate Pauli put it a long time ago, 'While God has created solids as perfectly ideal crystals, the devil is responsible for their imperfect surfaces'. Of course, the simulations can make contact with this complex reality as well, putting into the model more and more of these non-ideal effects (which can again be varied in a controlled manner to check their relevance).

Of course, surfaces and interfacial effects are not only of great interest near critical points, but in a much wider context. Just as in an Ising ferromagnet we may ask how the magnetization $m_n$ varies as a function of the layer index $n$, in a fluid we may ask what is the profile of the local density $\rho(z)$ as function of the distance $z$ from a solid wall (due to a container for instance), etc. Further, if we model flexible macromolecules as self-avoiding random walks (see Chapters 3, 4), we may consider the adsorption of flexible macromolecules at a hard wall in terms of a model where a monomer adjacent to a wall wins an energy $\varepsilon$, and this enthalpic gain may outweigh the entropic loss due to the reduced number of SAW configurations near a wall (Binder, 1983).

While many of the technical aspects of simulations of models addressing the effects of free surfaces or other boundaries are rather similar to simulations targeted to sample bulk properties, where surface effects are deliberately eliminated by the use of periodic boundary conditions, sometimes the demands for computational resources become exorbitant, since large (mesoscopic rather than of atomic scale) lengths occur. A typical example is the phenomenon of 'wetting', i.e. when a saturated gas below the critical temperature is exposed to a wall, in which a fluid layer may condense at the wall without accompanying condensation in the bulk. In the ideal case (and in the thermodynamic limit) the thickness of this 'wet' layer at the wall is infinite at all temperatures above the wetting temperature $T_w$. Of course, this is true only in the absence of gravity, and the chemical potential of the gas $\mu_{gas}(T)$ must always be held at its coexistence value $\mu_{coex}(T)$ for gas–liquid phase coexistence. For non-zero $\Delta\mu = \mu_{coex}(T) - \mu_{gas}(T)$, a fluid layer may also condense, but it is not infinitely thick, $\ell_{wetting} \propto (\Delta\mu)^{-p_{co}}$ where $p_{co}$ is some exponent that depends on the character of the forces between the wall and the particles in the gas (Dietrich, 1988). The approach to the wet state (for $T > T_w$) where $\ell_{wetting} \to \infty$ as $\Delta\mu \to 0$ is called 'complete wetting'. On the other hand, if we approach the wetting transition for $\Delta\mu = 0$ varying $T$ and let $T_w$ approach from below, we may distinguish two situations: $\ell_{wetting}(T \to T_w)$ may approach a finite value at $T_w$ and then jump discontinuously to infinity ('first order wetting'); or $\ell_{wetting}$ may show a critical divergence, $\ell_{wetting} \propto (T_w - T)^{-p}$ where $p$ is another exponent ('critical wetting'). To avoid confusion we mention that for short range forces in $d = 3$ dimensions actually both exponents $p_{co}$, $p$ are zero (which implies logarithmic divergences).

Simulation of such wetting phenomena is very difficult: not only must the linear dimension perpendicular to the wall be very large, much larger than $\ell_{wetting}$, but also the linear dimension of the system in the directions parallel to the wall must be huge, since a very large correlation length $\xi_{\parallel} \propto \Delta\mu^{-\nu_{co}}$ or $\xi_{\parallel} \propto (T_w - T)^{-\nu}$ appears (where $\nu_{co}$, $\nu$ are exponents appropriate for 'complete wetting' or 'critical wetting', respectively). The occurrence of

this large length can be understood qualitatively by recalling the interpretation of wetting phenomena as 'interface unbinding transitions' (Dietrich, 1988): as the fluid layer at the wall gets thicker, the gas–liquid interface gets more and more remote from the wall, and capillary wave excitations of larger and larger wavelength – up to $\xi_\parallel$ – become possible. This problem is very closely related to the finite size effects encountered in simulations set up to study interfaces between coexisting phases, already discussed in Section 4.2.3.6. Again the lesson is that a rather good qualitative understanding of the physics of a problem is already mandatory when one sets up the model parameters for a simulation of that problem.

Next we mention that even wetting phenomena can be studied with the simple Ising lattice model. We only have to remember the correspondence with the lattice gas interpretation: 'spin down' represents liquid, 'spin up' represents gas, and gas–liquid phase coexistence ($\Delta\mu = \Delta\mu_{\text{coex}}(T)$) in the Ising magnet then simply means that the bulk magnetic field $H$ is zero. A wetting transition can be induced by applying a negative surface field $H_1 < 0$ – hence favoring liquid at the wall – at the surface of a ferromagnet with a positive spontaneous magnetization (i.e. gas) in the bulk.

We now make some more specific comments on the technical aspects of the simulation of such systems and also present a few typical examples. If surface properties are of interest in a model for which the bulk values are well known, it may be preferable to sample layers near the surface more frequently than those far from the surface in order to reduce the statistical error in estimates for surface related properties. If the interior is sampled too infrequently, however, the bulk may not reach equilibrium, and this, in turn, will bias the surface behavior. If, instead, a slowly fluctuating interface is present, it may be preferable to sample layers in the interior, in the vicinity of the interface, more often than those near the surface. Both variants of preferential sampling have been used successfully; in a new problem it may be useful to first make some test runs before choosing the layer sampling probabilities. Note that there are a large number of interesting phenomena which may be seen in quite simple systems confined between two surfaces simply by varying the interaction in the surface layers and applying either surface or bulk fields, or both (see e.g. Landau, 1996; Binder and Landau, 1988, 1992; Binder *et al.*, 1989, 1996). Perhaps the simplest model which shows such effects is the $L \times L \times D$ Ising film with Hamiltonian

$$\mathcal{H} = -\mathcal{J} \sum_{\langle i,j \rangle \in \text{bulk}} \sigma_i \sigma_j - \mathcal{J}_{\text{s}} \sum_{\langle i,j \rangle \in \text{surf}} \sigma_i \sigma_j - H \sum_i \sigma_i - H_1 \sum_{i \in \text{surf}} \sigma_i, \quad (5.55)$$

which in the limit of $D \to \infty$ becomes equivalently a semi-infinite system with $L \times L$ surface. Thus, capillary condensation in thin films and layering and critical wetting in thick films have both been studied in simple nearest neighbor Ising models between two confining surfaces using preferential sampling. For example, the data for the layer magnetization, shown in Fig. 5.15, demonstrate quite clearly the onset of wetting as the surface field $H_1$ is varied. Perhaps the most interesting consequence of these studies is the discovery that

Fig. 5.15 Profiles of the layer magnetization for a $128 \times 128 \times 160$ Ising film with $\mathcal{J}_s/\mathcal{J} = 1.33$, $\mathcal{J}/k_B T = 0.226$. The arrows show the values of the bulk magnetization in the spin–up and spin–down phases. From Binder *et al.* (1989).
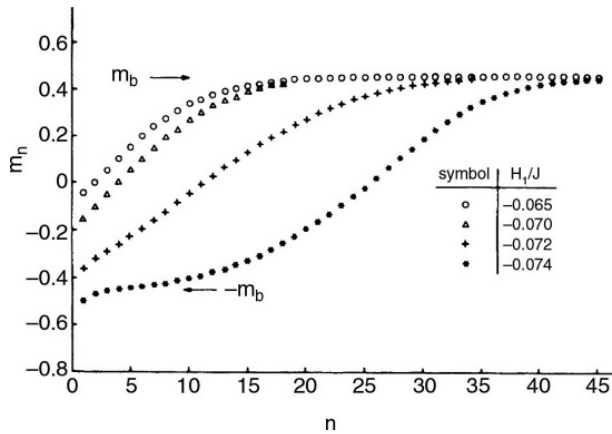


critical wetting is apparently mean-field-like in contradiction to theoretical predictions of non-universal, non-mean-field-like behavior. The discrepancy between the Monte Carlo result and the theoretical renormalization group calculation, which used as the characteristic length for the distance of the interface from the wall, was rather perplexing and helped spark new theoretical efforts. It currently appears likely that there is an additional characteristic length involved which renormalized the 'bare' result and that the simulational result was qualitatively correct (Boulter and Parry, 1995; Parry *et al.*, 2008). Extensive studies of these problems are still continuing (see, e.g., Pang *et al.*, 2011; Bryk and Binder, 2013) but they are still not yet fully resolved. The Monte Carlo data which yielded this unexpected result were not simple to obtain or analyze because of the large fluctuations to which we alluded earlier. For example, data for the suceptibility of $L \times L \times D$ systems with $L = 50, D = 40$ using standard Metropolis sampling showed huge fluctuations (see Fig. 5.16). When a multispin coding technique was used to make much longer runs with $L = 128, D = 80$, Fig. 5.16 shows that the results were much improved. Note, however, that even though these data were taken far from the transition, only roughly a factor of two increase in linear dimension was possible with an improvement of roughly $10^2$ in the implementation of the sampling algorithm.

Yet another simple variation in the choice of boundary conditions for a three-dimensional Ising model can produce 'wedge filling' instead of 'wetting' and yield entirely different physics. Instead of having two free, parallel surfaces as in the previous discussion, the situation portrayed in Fig. 5.17 effectively produced a double wedge geometry with a periodic boundary parallel to the wedges. In this case, critical wetting is supplanted by a transition that is analogous to the 'filling' transition that would occur in a single, infinite wedge. Here the corresponding 'thickness' is the distance from a corner, $l_0$, and this quantity diverges at the transition. The transition is characterized by fluctuations that are stronger than for the wetting transition and detailed Monte Carlo data (Milchev *et al.*, 2003a, 2003b) reveal critical exponents that differ from mean field values and agree with theoretical predictions. This is but
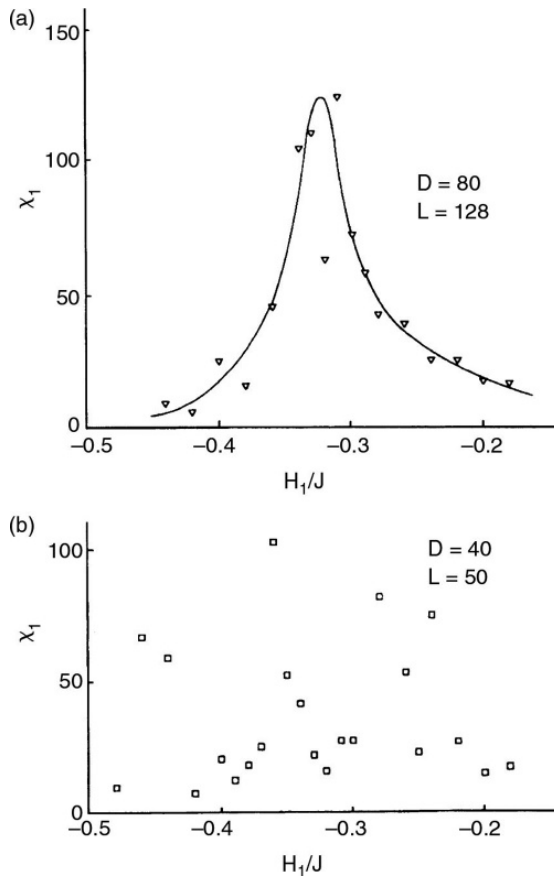
Fig. 5.16 Monte Carlo data for the surface layer suceptibility near the critical wetting transition of an Ising film for $\mathcal{J}_s = \mathcal{J}$, at $\mathcal{J}/k_B T = 0.23$. (a) Multispin coding data for $L = 128$, $D = 80$. (b) Metropolis data for $L = 50$, $D = 40$. From Binder et al. (1989).



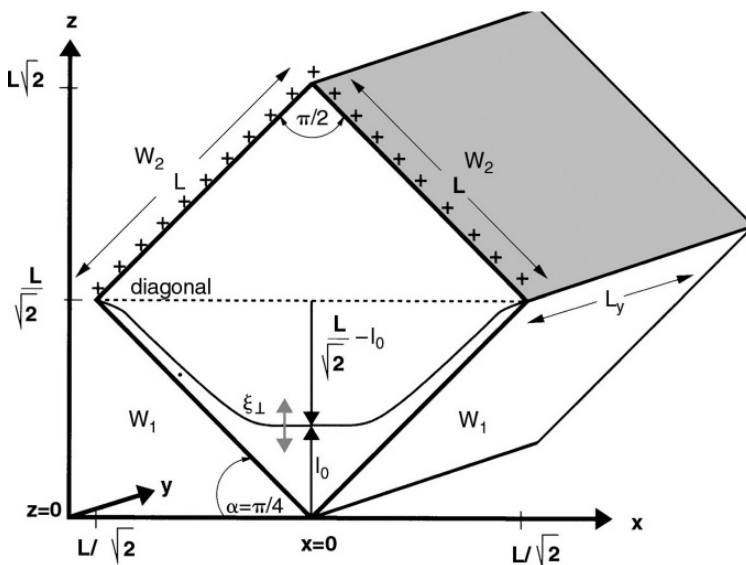Fig. 5.17 Sketch of the antisymmetric double wedge composed of surfaces $W_1$ and $W_2$ bounding an $L \times L \times L_y$ simple cubic Ising model. A periodic boundary condition is applied in the $y$-direction and magnetic fields of opposite sign, $\pm H_1$, act on the two different kinds of surfaces, $W_1$ and $W_2$, respectively. The position of the interface with respect to one corner is given by $l_0$.

one further example of how the clever use of boundary conditions makes new physical behavior accessible to Monte Carlo simulations. Since the correlation length $\xi_\perp$ for interfacial fluctuations normal to the interface (see Fig. 5.17) diverges less strongly than the correlation length $\xi y$ in the $y$-direction along the wedge, this geometry is another example where anisotropic finite size scaling (Binder and Wang, 1989) needs to be used.

A novel effect which occurs in interacting statistical systems between two walls is the 'Casimir effect'; an overview of this unusual but increasingly popular effect was given by Krech (1994). This effect is the equivalent of the phenomenon in electromagnetism in which a force is produced between two conducting plates separated by a vacuum due to quantum fluctuations in the electromagnetic field in the vacuum. The free energy of a system $\mathcal{F}$ at temperature $T$ and between plates of area $A$ and separated by a distance $D$ can be expressed as the sum of four terms,

$$\lim_{A \to \infty} \frac{\mathcal{F}(T, D)}{k_B T_{cb} A} = D F_{bulk}(T) + F_{s,a}(T) + F_{s,b}(T) + \delta F_{a,b}(T, D), \quad (5.56)$$

where $F_{s,a}$ and $F_{s,b}$ are surface free energies, and $\delta F_{a,b}$ is the finite separation contribution which in $d$-dimensions at the bulk critical point has a contribution ($\varepsilon = |1 - T/T_c|$)

$$\delta F_{a,b}^{sing}(\varepsilon = 0, D) = \Delta_{a,b} D^{-(d-1)}, \quad (5.57)$$

where $\Delta_{a,b}$ is the critical Casimir amplitude. The determination of the Casimir amplitude by simulations is quite difficult since it represents only a very small correction to the bulk and surface free energies. This has been done quite successfully by Krech and Landau (1996) using a variation of a method proposed by Mon (1985). As an example we consider two $L \times D$ square lattice systems: in the $x$-direction there are periodic boundary conditions for both systems, the second system is split into two horizontal strips, each of width $L$ and thickness $D/2$. The top strip has the same boundary conditions as the original lattice and the second one has periodic boundaries. An interaction $\lambda$ between the strips is used to interpolate between the two systems using umbrella sampling and the sums of different Casimir amplitudes are extracted from the difference. Using this scheme, however, there are finite size effects due to both $L$ and $D$ so an additional extrapolation is needed.

The behavior of the interface itself may be of interest. One well studied problem is that of interface roughening as the temperature is raised for a system which has a 'smooth' interface at low temperatures. (See, e.g., Ising model simulations by Mon *et al.* (1988, 1990).) At first glance it would seem that the simplest way to impose an interface would be by fixing the top and bottom walls of the system to point in opposite directions. As the interface roughness grows, however, it is possible that there will be excursions of the interface which will hit one of the walls; the 'confinement' of the interface may thus modify its behavior. Instead an antiperiodic boundary may be imposed so that the interface may wander in an unrestricted manner. A periodic boundary may then be used in the directions parallel to the interface (see Fig. 4.11). The

interfacial fluctuations may be quite slow and correlation times become quite long for large systems. An 'interface flipping' method has been developed by Hasenbusch and Meyer (1991) for the treatment of interfaces in solid-on-solid models. The essential ingredient in this method is that the entire interface is simply reflected about the mean interface position. This approach has been shown to greatly reduce the correlation time for fluctuations involving the interface near the roughening transition. For the three-dimensional Ising model they found an effective dynamic critical exponent of about 0.4 whereas Metropolis yields $z \sim 2$. Swendsen–Wang updating is even worse than local updating.

### 5.9.2 Anisotropic critical phenomena: simulation boxes with arbitrary aspect ratio

We have already encountered numerous cases where the results of a simulation depended on the size of the simulation box that often was taken as $L \times L$ (for a square lattice) or $L \times L \times L$ (for a simple cubic lattice). Studying the dependence of the results on the linear dimensions $L$ then turned out to be a useful way of understanding the macroscopic properties of the model system under consideration. In fact, the theoretical description of such finite size effects in terms of the finite size scaling theory (Section 4.2) has aided our understanding of such diverse problems as percolation (Section 3.6), static and dynamic critical behavior of Ising ferromagnets (Section 4.2), and spin glasses (Section 5.4). Later chapters will provide further examples (e.g. fluid phase coexistence in Section 6.1.4; melting in Section 6.1.5; polymer mixtures in Section 6.6; quantum models in Section 8.3.10; gelation in Section 10.5.2; phase transitions in lattice gauge theory in Sections 11.5, 11.7, and globular protein crystallization in Section 14.2). The typical problem for critical phenomena is that a characteristic length, the correlation length of order parameter fluctuations, $\zeta$, is much larger than all microscopic lengths (such as the lattice spacing when dealing with a lattice model). Then the main consequence of finite size effects is that one must consider properties as a function of the ratio $L/\zeta$.

However, this is not the whole story. When anisotropic critical phenomena occur there are *two* correlation lengths, $\zeta_{\parallel}$, $\zeta_{\perp}$, that describe the growth of correlations of the order parameter fluctuations in two different directions in space. For bulk critical phenomena the 'standard' example for such a situation is a special multicritical point, the so-called 'Lifshitz point'. Such points are found in the parameter space of certain models, e.g. an Ising model with an antiferromagnetic, next-nearest neighbor exchange $\mathcal{J}_2$ in the $z$-direction in addition to the nearest neighbor ferromagnetic exchange $\mathcal{J}_1$. In this so-called 'axial next nearest neighbor Ising' (ANNNI) model (Selke, 1988) a transition from the paramagnetic to the ferromagnetic phase occurs at $T_c(\kappa)$ for $\kappa \equiv -\mathcal{J}_2/\mathcal{J}_1 < \kappa_L$, while for $\kappa > \kappa_L$ there is a transition to a modulated phase. When the multicritical point $\kappa = \kappa_L$ is approached (Hornreich *et al.*, 1975), the correlation length $\zeta_{\parallel}$ in the $z$-direction exceeds the correlation length

$\zeta_\perp$ in the transverse direction(s). Even the corresponding critical exponents $\nu_{||}$, $\nu_\perp$ differ,

$$\zeta_{||} \propto \varepsilon^{-\nu_{||}}, \quad \zeta_\perp \propto \varepsilon^{-\nu_\perp}, \tag{5.58}$$

where $\varepsilon = T/T_L - 1$ with $T_L \equiv T_c(\kappa_L)$, and the critical exponents satisfy a generalized hyperscaling relation (cf. Eqs. (2.37) and (2.38)). Instead of $d\nu = \gamma + 2\beta$ ($d =$ dimensionality, $\gamma$ and $\beta$ being the critical exponents of susceptibility and order parameter (see Chapter 2)), we now have

$$(d-1)\nu_\perp + \nu_{||} = \gamma + 2\beta. \tag{5.59}$$

Before we explore the consequences of Eqs. (5.58) and (5.59) for the finite size scaling analysis of simulation data, we mention other examples of anisotropic criticality. A now well-understood example is critical wetting in the semi-infinite Ising square lattice with nearest neighbor interaction $\mathcal{J}$ and a surface magnetic field $H_1 < \mathcal{J}$ acting at the free surface. The bulk magnetic field is zero, the system is below its critical temperature $T_c$, and the sign of $H_1$ is opposite to the sign of the spontaneous magnetization in the bulk. Then, a critical wetting transition occurs at $T_w(H_1) < T_c$, where a macroscopically thick domain (with magnetization direction parallel to the surface field) forms adjacent to the free surface, separated from the bulk by an interface. As $T$ tends to $T_w(H_1)$ from below, a gradual 'interface unbinding' from the wall occurs. Such a one-dimensional interface, weakly bound to the wall, is a strongly fluctuating object. It resembles a self-avoiding random walk but is constrained by the periodic boundary condition in the direction parallel to the free surface. This interface fluctuates around its mean distance $\ell(T)$ from the free surface, and the fluctuations are again characterized by Eqn. (5.58), where $\zeta_{||}$ describes correlations of interfacial fluctuations in the direction parallel to the free surface, and $\zeta_\perp$ perpendicular to it. For this case, the exact solution is known (Abraham, 1986): $\nu_{||} = 2$, $\nu_\perp = 1$.

Our third example is a strongly anisotropic, non-equilibrium phase transition that occurs in Ising models with 'friction' (Hucht, 2009; Saracco and Gonella, 2009; Winter *et al.*, 2010; Angst *et al.*, 2012). There, one again considers an Ising model on the square lattice, choosing an $L_{||} \times L_\perp$ rectangular geometry with periodic boundary condition in the $x$-direction, but all rows are moved relative to each other. The time-dependent displacement $\Delta(t) = \upsilon t$ is equal relative to all adjacent rows, and one can interpret the 'velocity' $\upsilon$ as a shear rate for the modeling of phase separation in sheared fluids (Onuki, 1997). Within a Monte Carlo context, a shearing step is realized by randomly choosing a row parallel to the $x$-direction (which has index $n$ with $1 \leq n \leq L_\perp$) and, subject to a Metropolis acceptance criterion, all spins to the rows from $n$ to $L_\perp$ are shifted by one lattice unit in the $+x$-direction. At this point, we mention that a modification of the standard periodic boundary condition is used in the $y$-direction, namely an appropriately shifted periodic boundary condition is used to remove any discontinuity when going across the boundary. This trick is simply taken from Non-equilibrium Molecular Dynamics (NEMD) techniques (Lees and Edwards, 1972). In this problem, the critical point is shifted with increasing velocity (or shear rate, respectively) away

from its exactly known value, resulting in strongly anisotropic critical behavior (Winter *et al.*, 2010). In the limit of $\upsilon \to \infty$ one can show that $\nu_{||} = 3/2$ and $\nu_\perp = 1/2$ (Hucht, 2009; Angst *et al.*, 2012). A similar anisotropy of critical exponents is also believed to occur for another version of a non-equilibrium Ising model, namely the driven lattice gas (see Section 10.2), but there the situation still is rather controversial.

When we address the question of how such phenomena can be studied within a finite size scaling framework (see Section 4.2.3), which for isotropic systems was based on the principle 'the linear dimension $L$ scales with the correlation length $\zeta_{||}$', we naturally expect to have two scaling variables $L_{||}/\zeta_{||}$, $L_\perp/\zeta_\perp$. However, instead of $L_\perp/\zeta_\perp$, it is preferable to use another scaling variable $Y = (L_\perp/\zeta_\perp)(\zeta_{||}/L_{||})^{\nu_\perp/\nu_{||}} \propto L_\perp/L_{||}^{\nu_\perp/\nu_{||}}$ (Binder and Wang, 1989). If $\nu_{||} = \nu_\perp$, this variable is simply the 'aspect ratio' $L_\perp/L_{||}$ of the $L_{||} \times L_\perp$ simulation box. For this reason, the variable $L_\perp/L_{||}^{\nu_\perp/\nu_{||}}$ is called the 'generalized aspect ratio' of the system. The standard finite size scaling relations, as written in Eqn. (4.10), are then easily generalized, e.g. the susceptibility becomes

$$\chi = L^{\gamma/\nu_{||}} \chi^o (L_\perp/L_{||}^{\nu_\perp/\nu_{||}}, \varepsilon L_{||}^{1/\nu_{||}}). \tag{5.60}$$

Thus, the finite size scaling 'data collapse' for different $\varepsilon$ and $L_{||}$ survives if we vary both $L_{||}$ and $L_\perp$ such that the generalized aspect ratio is held constant. Then, the critical point can also be located by looking for intersection points of the fourth order cumulant $U_4$ (Eqn. (4.12)) in the usual way. Of course, the exponents $\nu_{||}$, $\nu_\perp$ are usually not known beforehand, and then varying $L_{||}$, $L_\perp$ to keep the generalized aspect ratio fixed is challenging. This problem has seriously hampered the study of all non-equilibrium Ising models.

Only in the case of critical wetting in $d = 2$ dimensions is the problem simpler, since there additional arguments show (Albano and Binder, 2012) that Eqn. (5.59) applies with an order parameter exponent $\beta = 0$. Hence, using $\nu_\perp = 1$ and $\nu_{||} = 2$ we find that the susceptibility exponent becomes $\gamma = 3$, and Eqn. (5.60) can be verified without the need to 'fit' any values for critical exponents. Using such concepts, wetting transitions in the two-dimensional Blume–Capel model (a three-state model with Ising spins $S_i = +1, 0, -1$ and a term proportional to $(S_i)^2$ in the Hamiltonian) could be successfully studied (Albano and Binder, 2012).

Unfortunately, critical wetting in $d = 3$ dimensions, where $\ell(T) \propto \ln(T - T_w)$ and $\zeta_\perp \propto (\ell(T))^{1/2}$, is much harder to explore; and, at the time of writing, a conclusive resolution of the problems discussed in the previous subsection still is not yet available.

### 5.9.3 Other Monte Carlo schemes

#### 5.9.3.1 Damage spreading

An example of a method which uses existing simulation techniques in a novel way is that of 'damage spreading' (Herrmann, 1990). (This phenomenon was first observed in cellular automata.) Two initial states of the system are prepared

in such a way that they differ only slightly. Both systems are then simulated with the same algorithm and the same random number sequence and the difference between the two systems, or the 'damage' is monitored to see if it disappears, stays about the same, or spreads; the spreading of the damage is an indication of the onset of a phase transition. A useful quantitative metric is given by the 'Hamming distance'

$$\Delta(t) = \frac{1}{2N} \sum_i |\sigma_i(t) - \rho_i(t)|, \tag{5.61}$$

where $\{\sigma_i(t)\}$ and $\{\rho_i(t)\}$ are the two 'parallel' time-dependent configurations and $N$ is the number of sites. The dynamical behavior will then be determined 'chaotic' if $\Delta(t)$ goes to a finite value as $t \to \infty$ for $\Delta(0) \to 0$. Studies on the Ising model show that the Hamming distance goes nicely to zero at the critical point. This is an example of a process which cannot be studied theoretically but is quite well suited for Monte Carlo simulation and delivers information in a quite unusual way. One interesting consequence of this process is that it shows that in multilattice coding it can be dangerous to adopt the time saving practice of using the same random number for every lattice if all the lattices are at the same temperature; except exactly at the critical point, all the lattices will eventually reach the same state.

### 5.9.3.2 Gaussian ensemble method

Challa and Hetheringon (1988) introduced a 'Gaussian ensemble' method which interpolates between the canonical and microcanonical ensemble. A system of $N$ spins is coupled to a bath of $N'$ spins which has a particular functional form for the entropy. (For $N' = 0$ the microcanonical is obtained, for $N' = \infty$ the canonical ensemble results.) The total, composite system is then simulated with the result that 'van der Waals loops' can be traced out clearly in $(E, T)$ space and the small system acts in many ways as a probe. The relative probability of two different states $\nu$ and $\mu$ is given by

$$\frac{P_\nu}{P_\mu} = \frac{\exp[-a(E_\nu - E_t)^2]}{\exp[-a(E_\mu - E_t)^2]}, \tag{5.62}$$

where $E_t$ is the total energy of the system plus bath and $a \propto 1/N'$. This method may offer certain advantages for the study of first order transitions, but more careful finite size analyses, considering both the size of the system as well as that of the heat bath, still need to be performed. We mention this approach here because it provides an example of how the theoretical concepts of reservoirs and walls, etc. can be used to develop a simple, new simulation technique with properties that differ from their more obvious predecessors.

### 5.9.3.3 Simulations at more than one length scale

Monte Carlo methods can also be used in concert with techniques that work at a different length scale. For example, Reuter *et al.* (2005) have shown that it can

be effective to use density functional theory (DFT) together with Monte Carlo for the study of phase transitions in adsorbed monolayers, e.g. O/Ru(0001). The DFT calculations provide effective interaction parameters for a grand canonical Monte Carlo simulation which in turn allows the determination of a phase diagram that includes multiple ordered phases. At least two of the ordered phases were later found experimentally, a finding that suggests that this approach has predictive value. This DFT/MC technique is but one example of the utility of combining diverse methods, and more will be said in this regard in Chapter 12. The extension of this approach to the study of adatom diffusion on surfaces has already been mentioned in Section 4.4.4.

### 5.9.4 Inverse and reverse Monte Carlo methods

Inverse Monte Carlo methods have been developed to calculate interaction energies from experimentally generated data for the short range order of a system (Gerold and Kern, 1987). In the original approach for $A$–$B$ binary alloys a 'model crystal' was created by starting with a random distribution of atoms with the correct concentration and determining the short range order coefficients. Then, a randomly chosen pair is exchanged if it reduces the sum of the squares of the deviations of the short range order coefficients. Once 'equilibrium' is obtained, the interaction parameters are then determined by looking at the fluctuations. Virtual exchanges are made and the number of $A$–$A$ bonds in each shell of neighbors is measured. This is done many times, and from the mean values of these bond numbers and the exchange probability expressed in terms of the energy change that would result, a set of equations, one for each shell of neighbors, is determined. These are then solved to extract estimates for the interaction energies. The method appears to be robust, i.e. a model with a given set of interactions can be simulated, and the resultant correlations can be used as input for an inverse Monte Carlo study. Such tests have been carried out successfully and interactions were determined for $Cu$–$Ni$, $Cu$–$Pt$ and $Cu$–$Au$ alloys.

Inverse Monte Carlo methods are also effective for the estimation of effective pair potentials for suitable off-lattice models. This is generally done using experimental scattering data of fluids and macromolecules (see e.g. Bathe and Rutledge, 2003) although in some test cases the target 'data' are generated by standard Monte Carlo or by molecular dynamics methods. (See Chapter 6 for more information about Monte Carlo simulations of off-lattice systems.) A quite efficient inverse Monte Carlo procedure, inspired by Wang–Landau sampling (see Section 7.8), was used with considerable success by Almarza and Lomba (2003) to extract estimated interaction parameters for liquid aluminum.

A closely related method, reverse Monte Carlo (McGreevy, 2001) differs from inverse Monte Carlo in that it does not attempt to generate an interaction Hamiltonian but only tries to reproduce the configuration that best reproduces experimental data for the pair distribution function. McGreevy (2001) outlines the 'details' of the method and presents a critical assessment of the quality of results that can be expected. His examples include the application to liquids,

Fig. 5.18 Application of the reverse Monte Carlo method to a two–dimensional Lennard–Jones system. On the left is the development of the radial distribution function. The dotted curves give the target 'data' (obtained by the Metropolis method) and the solid curves show the instantaneous distributions obtained from intermediate particle configurations (shown on the right). After McGreevy (2001).
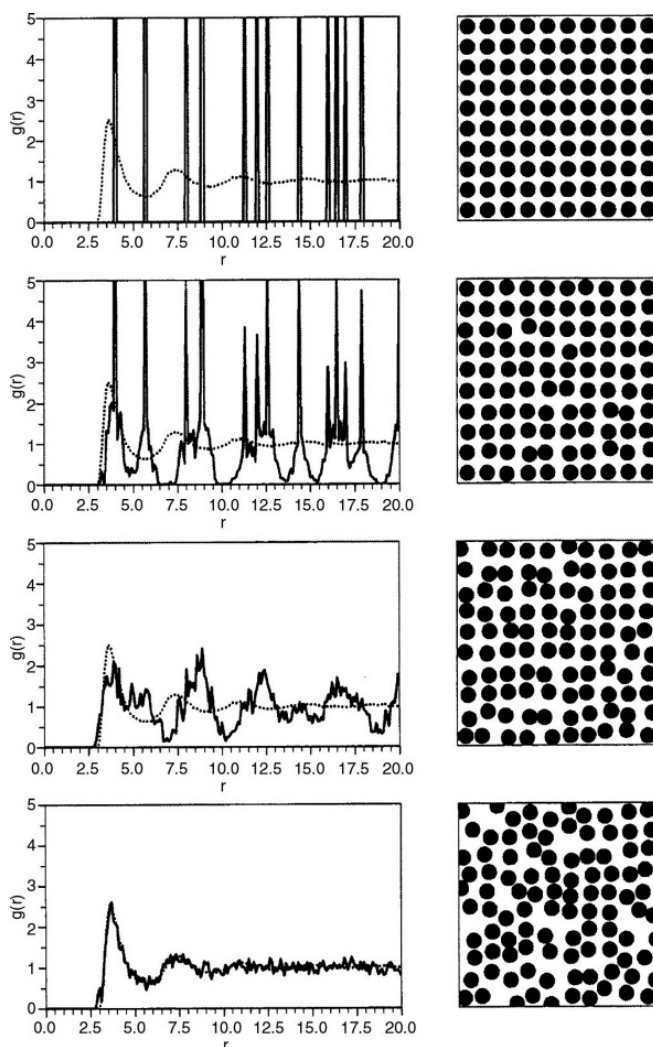
glasses, disorder in crystals, and magnetic structures. One quite instructional example is the description of a reverse Monte Carlo simulation for a small two–dimensional Lennard–Jones system (see Fig. 5.18). The initial state is a perfect crystal and the pair correlation function to which the intermediate values are being fitted (generated by Metropolis Monte Carlo) is shown by the dotted line. After 2500 trial moves are accepted, the distribution function has 'converged'. Of course, the target 'data' are themselves somewhat noisy and the ultimate accuracy will depend on the 'details' of the simulation, but the sequence shown in Fig. 5.18 shows clearly how the approach to the final state and the agreement between the simulated and target distribution functions are correlated. Developments in reverse Monte Carlo continue, and an extension of the original reverse Monte Carlo algorithm to produce dynamical models based on dynamical data has now been developed. A nice overview of the status

of the reverse Monte Carlo method can be found in the *Proceedings of the 3rd Workshop on Reverse Monte Carlo Methods* (Keen and Pusztai, 2007).

### 5.9.5  Finite size effects: review and summary

We have already seen a number of different cases where the finite system size affects the nature of the results. This may come about because of a discretization of the excitation spectrum in a classical system or due to a limitation of the correlation length near a phase transition in any system. In the latter case a cursory inspection of the data may be incapable of even determining the order of the transition, but we have seen that finite size scaling provides a theoretically well grounded mechanism for the extraction of system behavior in the thermodynamic limit. We have now observed multiple finite size scaling forms and have seen that they are clearly effective. The general feature of all of them is that if appropriate scaling variables are chosen, both the location of the transition temperature as well as a description of the behavior in the infinite system can be accurately extracted. Thus, for example, near a second order phase transition that is reached by changing the temperature, the appropriate scaling variable is $\varepsilon L^{1/\nu}$ as long as the lattice dimension is below the upper critical dimension. If instead the transition is approached by varying a field $h$ that is conjugate to the order parameter, the scaling variable is $hL^{\beta\delta/\nu}$. The complication in all of this is that as the size of the system increases, statistical errors become a problem because of correlations. Thus, the two effects of finite system size and finite sampling time become intertwined. For a temperature-driven first order transition the relevant scaling variable becomes $\varepsilon L^d$ where $d$ is the spatial dimension. In all cases, however, scaling is valid only in some asymptotic size regime which may vary from model to model. There have also been attempts to recast finite size scaling in a form which will enable the extraction of thermodynamic information at much longer size scales. Kim (1993) proposed using the ratio of the finite lattice correlation length and the lattice size as a new scaling variable and Kim *et al.* (1996) showed that, close enough to the phase transition of the Ising model, the behavior for lattices which were much larger than those which could be measured was accurately predicted.

In summary, then, the key to a successful finite size scaling analysis is the careful examination of the quality of the scaling with particular care given to the identification of systematic deviations (however small) from scaling. This means that the statistical accuracy of the data is important and some compromise must be made between large lattices and high statistics.

### 5.9.6  More about error estimation

In Chapter 2 we introduced simple concepts of the estimation of errors in Monte Carlo data, but these were based largely upon the assumption of a Gaussian distribution of the parent data population. More advanced methods of statistical analysis exist, but many of these rely on knowledge of what the

actual distribution is. In the general case, however, we do not know what the form of the parent distribution is or what biases or correlations are included in the data. There are, however, several more sophisticated approaches that sometimes fall under the rubric of 'resampling methods' and that do not require such knowledge. (These are also sometimes referred to as 'non-parametric estimation' techniques.)

One such more sophisticated method of error estimation, the 'jackknife', was introduced by Quenouille and Tukey (see, e.g., Miller, 1974) to reduce bias in an estimator and to provide a measure of the variance of the resulting estimator by reusing the individual values in the sample. This method, which has its origin in the theory of statistics, is of quite general applicability. Let $A_1 \ldots A_n$ represent a sample of $n$ independent and identically distributed random variables, where $<A>$ is the estimator calculated using all members of the sample. The data are divided into $g$ groups of size $h$ each, i.e. $n = gh$. Deleting the $k$th group of $h$ values, in turn, one then calculates mean jackknife data values $A_k^{JK}$ for the remaining data, i.e.

$$\overline{A}^{JK} = \frac{1}{g} \sum_{j=1}^{g} A_j^{JK}, \tag{5.63a}$$

where

$$A_j^{JK} = <A> - \frac{1}{h} \sum_{k=(j-1)h+1}^{k=j\,h} A_k. \tag{5.63b}$$

The jackknife estimate for the variance is then given by

$$V^{JK} = \frac{g-1}{g} \sum_{k=1}^{g} \left( A_k^{JK} \frac{1}{g} \sum_{j=1}^{g} A_k^{JK} \right)^2. \tag{5.64}$$

This estimate for the variance eliminates the order $n^{-1}$ bias from the estimator and provides a more realistic error estimate for data sets that contain bias. In the simplest case, $g = n$, and a single data point is eliminated from each jackknife data point; but even more sophisticated variants of the 'general' jackknife approach outlined above also exist. For more practical guidance on the use of simple jackknife procedures, the reader is referred elsewhere (Berg, 2004).

Another useful, and yet more general, statistical resampling approach to error estimation, developed by Efron (see, e.g., Miller, 1974), is the 'bootstrap' method. If there are originally $n$ data points in the data set, a number of 'new' data sets are created by randomly drawing $h$ values from the existing data $g$ times and then calculating the errors in the traditional way using the $g$ new samples. A data point from the original data set may be drawn more than once for inclusion in a new data set. The bootstrap approach works well in the limit of a large value of $g$, but may not yield reliable error estimates if $g$ is small. The 'smoothed bootstrap' variation, i.e. the kernel density approach, also assigns a small amount of random noise to each choice of data point drawn from the

original sample. The bootstrap method is quite simple to apply, but there is no obvious choice for the number of randomly drawn samples that should be used.

A general 'rule of thumb' to follow in deciding on error bars is that when jackknife, bootstrap, or simple error estimates disagree, choose the least optimistic one. Of course, all such estimates need to be made with care, because an unrealistically large error bar will diminish the practitioner's ability to draw conclusions about the physical behavior that may be contained in the data.

### 5.9.7 Random number generators revisited

In Chapter 2 we briefly touched on the entire matter of random number generation and testing for quality. We now wish to return to this topic and cite a specific example where the deficiencies of several generators could only be clearly seen by careful inspection of the results of a Monte Carlo simulation which was carried out using the generator in question. The Wolff cluster flipping algorithm was used to study $16 \times 16$ Ising square lattices using the generators defined in Chapter 2. Most of the simulations were performed exactly at $T = T_c$, and between five and 10 runs of $10^7$ updates were performed. (Note that for the Swendsen–Wang and Metropolis algorithms, one update means one complete update of the lattice (MCS); in the Wolff algorithm, one update is less than one MCS and depends on the temperature. For simulations at $T_c$, a Wolff update is ~0.55 MCS.) Surprisingly, the use of the 'high quality' generators together with the Wolff algorithm produces *systematically incorrect* results. Simulations using R250 produce energies which are systematically too *low* and specific heats which are too *high* (see Table 5.1). Each of the 10 runs was made at the infinite lattice critical temperature and calculated averages over $10^6$ MCS; the deviation from the exact value of the energy was over $40\sigma$ (standard deviations)! Runs made using the SWC generator gave better results, but even these data showed noticeable systematic errors which had the opposite sign from those produced using R250. In contrast, data obtained using the simple 32 bit congruential generator CONG produced answers which were correct to within the error bars. Even use of the mixed generator SWCW did not yield results which were free of bias, although the systematic errors were much smaller ($2\sigma$ for the energy and $4\sigma$ for the specific heat). Use of another shift-register random number generator, R1279, resulted in data which were in substantially better agreement with exact values than were the R250 values. These data may be contrasted to those which were obtained using the identical random number generators in conjunction with the single spin-flip Metropolis method and the multicluster flipping approach of Swendsen and Wang (1987). For all combinations of simulation methods and random number generators, the energy and specific heat values (shown in Table 5.2) are correct to within a few $\sigma$ of the respective simulations; except for the CONG generator with Metropolis and R250 with Swendsen–Wang, the answers agree to within $1\sigma$.

The problems which were encountered with the Wolff method are, in principle, a concern with other algorithms. Although Metropolis simulations are

Table 5.1 *Values of the internal energy for 10 independent runs with the Wolff algorithm for an $L = 16$ Ising square lattice at $K_c$. The last number in each column, labeled 'dev', gives the difference between the simulation value and the exact value, measured in terms of the standard deviation $\sigma$ of the simulation.*

|  | CONG | R250 | R1279 | SWC | SWCW |
|---|---|---|---|---|---|
|  | 1.453 089 | 1.455 096 | 1.453 237 | 1.452 321 | 1.453 058 |
|  | 1.453 107 | 1.454 697 | 1.452 947 | 1.452 321 | 1.453 132 |
|  | 1.452 866 | 1.455 126 | 1.453 036 | 1.452 097 | 1.453 330 |
|  | 1.453 056 | 1.455 011 | 1.452 910 | 1.452 544 | 1.453 219 |
|  | 1.453 035 | 1.454 866 | 1.453 040 | 1.452 366 | 1.452 828 |
|  | 1.453 198 | 1.455 054 | 1.453 065 | 1.452 388 | 1.453 273 |
|  | 1.453 032 | 1.454 989 | 1.453 129 | 1.452 444 | 1.453 128 |
|  | 1.453 169 | 1.454 988 | 1.453 091 | 1.452 321 | 1.453 083 |
|  | 1.452 970 | 1.455 178 | 1.453 146 | 1.452 306 | 1.453 216 |
|  | 1.453 033 | 1.455 162 | 1.452 961 | 1.452 093 | 1.453 266 |
| $-<E>$ | 1.453 055 | 1.455 017 | 1.453 056 | 1.452 320 | 1.453 153 |
| error | 0.000 030 | 0.000 046 | 0.000 032 | 0.000 044 | 0.000 046 |
| dev. | $-0.31\,\sigma$ | $42.09\,\sigma$ | $-0.27\,\sigma$ | $-16.95\,\sigma$ | $1.94\,\sigma$ |

Table 5.2 *Values of the internal energy (top) and specific heat (bottom) for an $L = 16$ Ising square lattice at $K_c$. Data were obtained using different random number generators together with Metropolis and Swendsen–Wang algorithms. The values labeled 'dev.' show the difference between the simulation results and the exact values in terms of standard deviations $\sigma$ of the simulations.*

|  | Metropolis CONG | SW CONG | Metropolis R250 | SW R250 | Metropolis SWC | SW SWC |
|---|---|---|---|---|---|---|
| $-\langle E\rangle$ | 1.452 783 | 1.453 019 | 1.453 150 | 1.452 988 | 1.453 051 | 1.453 236 |
| error | 0.000 021 | 0.000 053 | 0.000 053 | 0.000 056 | 0.000 080 | 0.000 041 |
| dev. | $-13.25\sigma$ | $-0.86\sigma$ | $1.62\sigma$ | $-1.36\sigma$ | $-0.17\sigma$ | $4.16\sigma$ |
| $-\langle C\rangle$ | 1.497 925 | 1.498 816 | 1.498 742 | 1.496 603 | 1.498 794 | 1.499 860 |
| error | 0.000 179 | 0.000 338 | 0.000 511 | 0.000 326 | 0.000 430 | 0.000 433 |
| dev. | $-4.40\sigma$ | $0.31\sigma$ | $0.06\sigma$ | $-6.47\sigma$ | $0.19\sigma$ | $2.65\sigma$ |

not as sensitive to these correlations, as resolution improves some very small bias may appear. In fact, some time after the errors with the Wolff algorithm were first noticed, a separate simulation of the Blume–Capel model (spin-1 Ising model with single ion anisotropy) near the tricritical point revealed asymmetries in the resultant distribution of states between $+1$ and $-1$, which with the Metropolis method were clearly traced to problems with the random

number generator (Schmid and Wilding, 1995). Hidden errors obviously pose a subtle, potential danger for many simulations such as percolation or random walks of various kinds which generate geometric structures using similar 'growth algorithms' as the Wolff method.

The problems with the widely used shift register generator have been attributed to triplet correlations (Heuer *et al.*, 1997; Compagner, 1991). This problem can be simply removed by XORing together two shift register generators with different pairs of lags without too great a loss in speed. The 'universal' properties have been analyzed by Shchur and Butera (1998) and we refer the reader to this paper and to Heuer *et al.* (1997) for a deeper description of the problems and tests. We do wish to comment that it is nonetheless unclear just how and why these correlations affect specific algorithms in the manner that they do.

To summarize, extensive Monte Carlo simulations on an Ising model for which the exact answers are known have shown that ostensibly high quality random number generators may lead to subtle, but *dramatic*, systematic errors for some algorithms, but not others. Since there is no reason to believe that this model has any special idiosyncrasies, this result should be viewed as another stern warning about the need to test very carefully the implementation of new algorithms. In particular, each specific algorithm must be tested together with the random number generator being used *regardless* of the tests that the generator has previously passed.

Mertens and Bauke (2004) re-examined the connection between random number sequence limitations and the Wolff algorithm as applied to the Ising model. They found a correlation between the bias of several lagged Fibonacci generators and the average cluster size and suggested the use of a hybrid congruential lagged Fibonacci generator that had good 'entropic' characteristics. This generator is much faster than the RANLUX generator (Lüscher, 1994) often used in high energy physics which discards many random numbers that are generated. A different approach was taken by Plascak *et al.* (2002) who mixed Wolff cluster flips and Metropolis single spin-flips in a single simulation. With the addition of ~50% of Metropolis flips the systematic error in the simulation of the Ising square lattice with R250 was essentially eliminated. Somewhat surprisingly, the relative performance was also enhanced even though the correlation times of the Metropolis algorithm *exceed* those of the Wolff algorithm.

Recently, a method of generating random number sequences of high quality with very long periods using the Sinai–Arnold map or cat-map was proposed by Barash and Shchur (2006). They show that introducing hidden variables and rotation in the random number generator output can dramatically suppress correlations. They also provide a table of results of various statistical tests as well as for periods and computational speeds for different advanced generators. This rather novel approach to random number generation is not necessarily more time consuming than other 'very high quality' generators and suggests that limitations in random number generators may continue to be overcome by the development of new, inventive algorithms.

Fig. 5.19
Approximate variation
of Ising model
simulation
performance with
time: (upper curve)
total relative
performance; (lower
curve) relative
improvement in
computer speed.
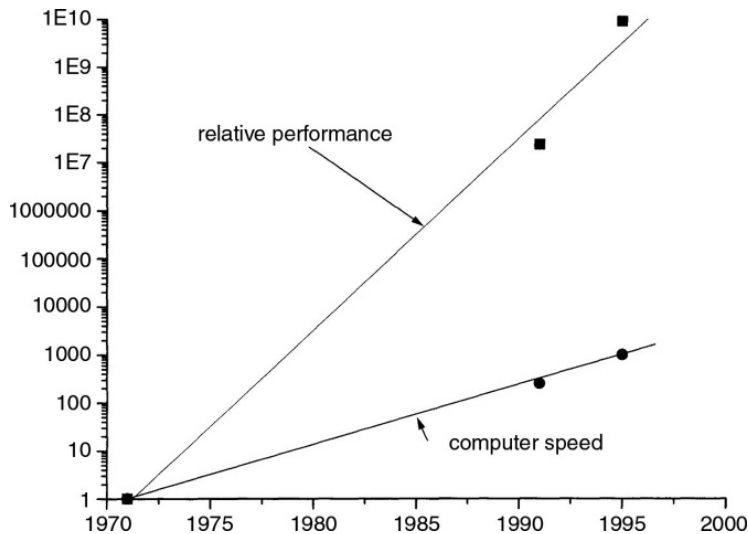


Thus, our understanding of and cures for random number 'diseases' are continuing to progress, but as computers continue to increase in performance and Monte Carlo runs use ever more random numbers, the practitioner must remain cautious.

The recent developments in computer hardware have consequences for random number production. Because of the movement towards massively parallel machines, the need to have reliable parallel random number generators has become an important topic. Manssen *et al.* (2012) present a nice overview on this topic for simulations on GPUs and Barash and Shchur (2013, 2014) offer an updated Fortran Program Library for parallel streams of random numbers. Lastly, Intel's Ivy Bridge processors contain a hardware random number generator based upon thermal noise. While slow compared to the digital pseudo–random number generators discussed earlier, it has the advantage of being a 'true' random number generator.

## 5.10 SUMMARY AND PERSPECTIVE

We have now seen a quite broad array of different simulational algorithms which may be applied to different systems and situations. Many new approaches have been found to circumvent difficulties with existing methods, and together with the rapid increase in computer speed the overall increase in our capabilities has been enormous. In fact, a brief overview of progress made for the Ising model over a 25-year period, shown in Fig. 5.19, indicates that the improvement due to algorithmic improvements far exceeds that due to raw computer speed alone. Of course, it is not only the improvement in speed which matters but also the net cost. Over the last decade alone the cost of purchasing a machine divided by the speed of the Monte Carlo algorithm has decreased by a factor of $10^4$! Ultimately, however, the choice of method depends on the

problem being considered, the type of computer which is available, and the judgement of the researcher.

## REFERENCES

Abraham, D. B. (1986), in *Phase Transitions and Critical Phenomena*, eds. C. Domb and J. L. Lebowitz (Academic Press, London), vol. 10, p. 1.

Adam, E., Billard, L., and Lancon, F. (1999), *Phys. Rev. E* **59**, 1212.

Albano, E. V. and Binder, K. (2012), *Phys. Rev. E* **85**, 061601.

Alexandrowicz, Z. (1975), *J. Stat. Phys.* **13**, 231.

Almarza, N. G. and Lomba, E. (2003), *Phys. Rev. E* **68**, 011202.

Angst, S., Hucht, A., and Wolf, D. E. (2012), *Phys. Rev. E* **85**, 051120.

Ballesteros, H. G., Cruz, A., Fernandez, L. A., Martin–Mayor, V., Pech, J., Ruiz-Lorenzo, J. J., Tarancon, A., Tellez, P., Ullod, E. L., and Ungil, C. (2000), *Phys. Rev. B* **62**, 14237.

Barash, L. and Shchur, L. N. (2006), *Phys. Rev. E* **73**, 036701.

Barash, L. Y. and Shchur, L. (2013), *Comput. Phys. Commun*. **184**, 2367.

Barash, L. Y. and Shchur, L. (2014), *Comput. Phys. Commun*. **185**, 1343.

Bathe, M. and Rutledge, G. C. (2003), *J. Comput. Chem.* **24**, 876.

Berg, B. (2004), *Markov Chain Monte Carlo Simulations and Their Statistical Analysis* (World Scientific, Singapore).

Berg, B. A. and Neuhaus, T. (1991), *Phys. Lett. B* **267**, 241.

Berg, B. A. and Neuhaus, T. (1992), *Phys. Rev. Lett.* **68**, 9.

Bhatt, R. N. and Young, A. P. (1985), *Phys. Rev. Lett.* **54**, 924.

Binder, K. (1977), *Z. Phys. B* **26**, 339.

Binder, K. (1983), in *Phase Transitions and Critical Phenomena*, Vol. VIII, eds. C. Domb and J. L. Lebowitz (Academic Press, London), p. 1.

Binder, K. and Kolb, W. (2011), *Glussy Materials and Disordered Solids*, 2nd edn. (World Scientific, Singapore).

Binder, K. and Landau, D. P. (1988), *Phys. Rev. B* **37**, 1745.

Binder, K. and Landau, D. P. (1992), *J. Chem. Phys.* **96**, 1444.

Binder, K. and Schröder, K. (1976), *Phys. Rev. B* **14**, 2142.

Binder, K. and Wang, J.-S. (1989), *J. Stat. Phys.* **55**, 87.

Binder, K. and Young, A. P. (1986), *Rev. Mod. Phys.* **58**, 801.

Binder, K., Landau, D. P., and Wansleben, S. (1989), *Phys. Rev. B* **40**, 6971.

Binder, K., Evans, R., Landau, D. P., and Ferrenberg, A. M. (1996), *Phys. Rev. E* **53**, 5023.

Bortz, A. B., Kalos, M. H., and Lebowitz, J. L. (1975), *J. Comput. Phys.* **17**, 10.

Boulter, C. J. and Parry, A. O. (1995), *Phys. Rev. Lett.* **74**, 3403.

Brown, F. R. and Woch, T. J. (1987), *Phys. Rev. Lett.* **58**, 2394.

Bryk, P., and Binder, K. (2013), *Phys. Rev. E* **88**, 030401(R).

Cardy, J. L. and Jacobsen, J. L. (1997), *Phys. Rev. Lett.* **79**, 4063.

Challa, M. S. S. and Hetherington, J. H. (1988), *Phys. Rev. Lett.* **60**, 77.

Chen, K., Ferrenberg, A. M., and Landau, D. P. (1993), *Phys. Rev. B* **48**, 3249.

Chen, S., Ferrenberg, A. M., and Landau, D. P. (1995), *Phys. Rev. E* **52**, 1377.

Compagner, A. (1991), *J. Stat. Phys.* **63**, 883.

Creutz, M. (1980), *Phys. Rev. D* **21**, 2308.

Creutz, M. (1983), *Phys. Rev. Lett.* **50**, 1411.

Creutz, M. (1987), *Phys. Rev. D* **36**, 515.

Crisanti, A. and Ritort, F. (2003), *J. Phys. A* **36**, R181.

de Miguel, E., Marguta, R. G., and del Rio, E. M. (2007), *J. Chem. Phys.* **127**, 154512.

De Meo, M., D'Onorio, M., Heermann, D., and Binder, K. (1990), *J. Stat. Phys.* **60**, 585.

Dietrich, S. (1988), in *Phase Transitions and Critical Phenomena*, Vol. XII, eds. C. Domb and J. L. Lebowitz (Academic Press, London), p. 1.

Dukovski, I., Machta, J., and Chayes, L. V. (2002), *Phys. Rev. E* **65**, 026702.

Dünweg, B. and Landau, D. P. (1993), *Phys. Rev. B* **48**, 14182.

Edwards, S. F. and Anderson, P. W. (1975), *J. Phys. F* **5**, 965.

Eisenbach, M., Zhou, C.-G., Nicholson, D. M., Brown, G., Larkin, J., and Schulthess, T. C. (2009), in *SC '09: Proceedings of the Conference on High Performance Computing Networking, Storage and Analysis* (Portland, Oregon).

Evertz, H. G. and Landau, D. P. (1996), *Phys. Rev. B* **54**, 12, 302.

Fortuin, C. M. and Kasteleyn, P. W. (1972), *Physica* **57**, 536.

Frenkel, D. and Ladd, A. J. C. (1984), *J. Chem. Phys.* **81**, 3188.

Fukui, K. and Todo, S. J. (2009), *Comput. Phys.* **228**, 2629.

Gerold, V. and Kern, J. (1987), *Acta. Metall.* **35**, 393.

Geyer, C. (1991), in *Proceedings of the 23rd Symposium on the Interface*, ed. E. M. Keramidas (Interface Foundation, Fairfax, Virginia), p. 156.

Goodman, J. and Sokal, A. (1986), *Phys. Rev. Lett.* **56**, 1015.

Griffiths, R. B. (1969), *Phys. Rev. Lett.* **23**, 17.

Hartmann, A. and Rieger, H. (2002), *Optimization Algorithms in Physics* (Wiley-VCH, Weinheim).

Hasenbusch, M. and Meyer, S. (1990), *Phys. Lett. B* **241**, 238.

Hasenbusch, M. and Meyer, S. (1991), *Phys. Rev. Lett.* **66**, 530.

Hasenbusch, M. (1995), *Nucl. Phys. B* **42**, 764.

Hatano, N. and Gubernatis, J. E. (1999) *AIP Conf. Proc.* **469**, 565.

Heermann, D. W. and Burkitt, A. N. (1990), in *Computer Simulation Studies in Condensed Matter Physics II*, eds. D. P. Landau, K. K. Mon, and H.-B. Schüttler (Springer Verlag, Heidelberg).

Heffelfinger, G. S. (2000), *Comput. Phys. Commun.* **128**, 219.

Herrmann, H. J. (1990), in *Computer Simulation Studies in Condensed Matter Physics II*, eds. D. P. Landau, K. K. Mon, and H.-B. Schüttler (Springer Verlag, Heidelberg).

Heuer, A., Dünweg, B., and Ferrenberg, A. M. (1997), *Comput. Phys. Commun.* **103**, 1.

Holm, C. and Janke, W. (1993), *Phys. Lett. A* **173**, 8.

Hornreich, R. M., Luban, M., and Shtrikman, S. (1975), *Phys. Rev. Lett.* **35**, 1678.

Hucht, A. (2009), *Phys. Rev. E* **80**, 061138.

Hui, K. and Berker, A. N. (1989), *Phys. Rev. Lett.* **62**, 2507.

Hukushima, K. and Nemoto, K. (1996), *J. Phys. Soc. Japan* **65**, 1604.

Hukushima, K. and Kawamura, H. (2000), *Phys. Rev. E* **61**, R1008.

Imry, Y. and Ma, S. (1975), *Phys. Rev. Lett.* **35**, 1399.

Kandel, D., Domany, E., Ron, D., Brandt, A., and Loh, Jr., E. (1988), *Phys. Rev. Lett.* **60**, 1591.

Kandel, D., Domany, E., and Brandt, A. (1989), *Phys. Rev. B* **40**, 330.

Kasteleyn, P. W. and Fortuin, C. M. (1969), *J. Phys. Soc. Japan Suppl.* **26s**, 11.

Katzgraber, H. G., Palassini, M., and Young, A. P. (2001), *Phys. Rev. B* **63**, 184422.

Kawashima, N. and Young, A. P. (1996), *Phys. Rev. B* **53**, R484.

Keen, D. A. and Pusztai, L., eds. (2007), *Proceedings of the 3rd Workshop on Reverse Monte Carlo Methods*, *J. Phys. Condens. Matter* **19**, issue 33.

Kim, J.-K. (1993), *Phys. Rev. Lett.* **70**, 1735.

Kim, J.-K., de Souza, A. J. F., and Landau, D. P. (1996), *Phys. Rev. E* **54**, 2291.

Kinzel, W. and Kanter, I. (2003), *J. Phys. A: Math. Gen.* **36**, 11173.

Kirkpatrick, S., Gelatt, Jr., S. C., and Vecchi, M. P. (1983), *Science* **220**, 671.

Kolesik, M., Novotny, M. A., and Rikvold, P. A. (1998), *Phys. Rev. Lett.* **80**, 3384.

Krech, M. (1994), *The Casimir Effect in Critical Systems* (World Scientific, Singapore).

Krech, M. and Landau, D. P. (1996), *Phys. Rev. E* **53**, 4414.

Landau, D. P. (1992), in *The Monte Carlo Method in Condensed Matter Physics*, ed. K. Binder (Springer, Berlin).

Landau, D. P. (1994), *Physica A* **205**, 41.

Landau, D. P. (1996), in *Monte Carlo and Molecular Dynamics of Condensed Matter Systems*, eds. K. Binder and G. Ciccotti (Società Italiana de Fisica, Bologna).

Landau, D. P. and Binder, K. (1981), *Phys. Rev. B* **24**, 1391.

Landau, D. P. and Krech, M. (1999), *J. Phys. Cond. Mat.* **11**, 179.

Laradji, M., Landau, D. P., and Dünweg, B. (1995), *Phys. Rev. B* **51**, 4894.

Lee, J. and Kosterlitz, J. M. (1990), *Phys. Rev. Lett.* **65**, 137.

Lee, L. W. and Young, A. P. (2003), *Phys. Rev. Lett.* **90**, 227203.

Lees, A. W. and Edwards, S. F. (1972), *J. Phys. C* **5**, 1921.

Luijten, E. and Blöte, H. W. J. (1995), *Int. J. Mod. Phys. C* **6**, 359.

Lüscher, M. (1994), *Comput. Phys. Commun.* **79**, 100.

Lyubartsev, A. P., Martsinnovski, A. A., Shevkunov, S. V., and Vorontsov-Velyaminov, P. N. (1992), *J. Chem. Phys.* **96**, 1776.

Machta, J., Choi, Y. S., Lucke, A., and Schweizer, T. (1995), *Phys. Rev. Lett.* **75**, 2792; (1996), Phys. Rev. E **54**, 1332.

Manssen, M., Weigel, M., and Hartmann, A. K. (2012), *Eur. Phys. J. Special Topics* **210**, 53.

Marinari, E. and Parisi, G. (1992), *Europhys. Lett.* **19**, 451.

Marsaglia, G. (1972), *Ann. Math. Stat.* **43**, 645.

McGreevy, R. L. (2001), *J. Phys.: Condens. Matter* **13**, R877.

Meirovitch, H. and Alexandrowicz, Z. (1977), *Mol. Phys.* **34**, 1027.

Mertens, S. and Bauke, H. (2004), *Phys. Rev. E* **69**, 055702(R).

Mézard, M. and Montanari, A. (2009), *Information, Physics and Computation* (Oxford University Press, Oxford).

Milchev, A., Müller, M., Binder, K., and Landau, D. P. (2003a), *Phys. Rev. Lett.* **90**, 136101.

Milchev, A., Müller, M., Binder, K., and Landau, D. P. (2003b), *Phys. Rev. E* **68**, 031601.

Miller, R. G. (1974), *Biometrika* **61**, 1.

Mon, K. K. (1985), *Phys. Rev. Lett.* **54**, 2671.

Mon, K. K., Wansleben, S., Landau, D. P., and Binder, K. (1988), *Phys. Rev. Lett.* **60**, 708.

Mon, K. K., Landau, D. P., and Stauffer, D. (1990), *Phys. Rev. B* **42**, 545.

Nadler, W. and Hansmann, U. H. E. (2007a), *Phys. Rev. E* **75**, 026109.

Nadler, W. and Hansmann, U. H. E. (2007b), *Phys. Rev. E* **76**, 609701.

Nadler, W. and Hansmann, U. H. E. (2008), *J. Phys. Chem. B* **112**, 10386.

Nishimori, H. (2001), *Statistical Physics of Spin Glasses and Information Processing: An Introduction* (Oxford University Press, Oxford).

Novotny, M. A. (1995a), *Phys. Rev. Lett.* **74**, 1.

Novotny, M. A. (1995b), *Computers in Physics* **9**, 46.

Ogielski, A. T. (1985), *Phys. Rev. B* **32**, 7384.

Onuki, A. (1997), *J. Phys.: Condens. Matter* **9**, 6119.

Pang, L., Landau, D. P., and Binder, K. (2011), *Phys. Rev. Lett.* **106**, 236102.

Parry, A. D., Rascón, C., Bernadino, N. R., and Romero-Enrique, J. M. (2008), *Phys. Rev. Lett.* **100**, 136105.

Polson, J. M., Trizac, E., Pronk, S., and Frenkel, D. (2000), *J. Chem. Phys.* **112**, 5339.

Plascak, J.-A., Ferrenberg, A. M., and Landau, D. P. (2002), *Phys. Rev. E* **65**, 066702.

Rampf, F., Paul, W., and Binder, K. (2005), *Europhys. Lett.* **70**, 628.

Reuter, K., Stampfl, C., and Scheffler, M. (2005), *Handbook of Materials Modeling*, ed. S. Yip (Springer, Berlin), vol. 1, p. 149.

Rosta, E. and Hummer, G. (2009), *J. Chem. Phys.* **131**, 165102.

Rosta, E. and Hummer, G. (2010), *J. Chem. Phys.* **132**, 034102.

Saracco, G. P. and Gonella, G. (2009), *Phys. Rev. E* **80**, 051126.

Sasaki, M. and Matsubara, F. (2008), *J. Phys. Soc. Japan* **77**, 024004.

Sasaki, M. (2009), *Phys. Rev. E* **82**, 031118.

Schilling, T. and Schmid, F. (2009), *J. Chem. Phys.* **131**, 231102.

Schmid, F. and Wilding, N. B. (1995), *Int. J. Mod. Phys. C* **6**, 781.

Schneider, J. J. and Kirkpatrick, S. (2006), *Stochastic Optimization* (Springer, Berlin).

Selke, W. (1988), *Phys. Repts.* **170**, 213.

Selke, W., Shchur, L. N., and Talapov, A. L. (1994), in *Annual Reviews of Computer Science I*, ed. D. Stauffer (World Scientific, Singapore) p. 17.

Shchur, L. N. and Butera, P. (1998), *Int. J. Mod. Phys. C* **9**, 607.

Sweeny, M. (1983), *Phys. Rev. B* **27**, 4445.

Swendsen, R. H. and Wang, J.-S. (1986), *Phys. Rev. Lett.* **57**, 2607.

Swendsen, R. H. and Wang, J.-S. (1987), *Phys. Rev. Lett.* **58**, 86.

Tipton, W. W., and Hennig, R. G. (2013), *J. Phys.: Condens. Matter* **25**, 495401.

Tomita, Y. and Okabe, Y. (2001), *Phys. Rev. Lett.* **86**, 572.

Tröster, A. (2007), *Phys. Rev. B* **76**, 012402.

Tröster, A. (2008a), *Phys. Rev. Lett.* **100**, 140602.

Tröster, A. (2008b), *Comput. Phys. Comm.* **179**, 30.

Tröster, A. (2013), *Phys. Rev. B* **87**, 104112.

Uhlherr, A. (2003), *Comput. Phys. Commun.* **155**, 31.

Wang, J.-S., Swendsen, R. H., and Kotecký, R. (1989), *Phys. Rev. Lett.* **63**, 109.

Wang, J.-S. (1989), *Physica A* **161**, 249

Wang, J.-S. (1990), *Physica A* **164**, 240.

Wansleben, S. (1987), *Comput. Phys. Commun.* **43**, 315.

Winter, D., Virnau, P., Horbach, J., and Binder, K. (2010), *Europhys. Lett.* **91**, 60002.

Wiseman, S. and Domany, E. (1995), *Phys. Rev. E* **52**, 3469.

Wiseman, S. and Domany, E. (1998), *Phys. Rev. Lett.* **81**, 22.

Wolff, U. (1988), *Nucl. Phys. B* **300**, 501.

Wolff, U. (1989a), *Phys. Rev. Lett.* **62**, 361.

Wolff, U. (1989b), *Nucl. Phys. B* **322**, 759.

Wolff, U. (1990), *Nucl. Phys. B* **334**, 581.

Young, A. P. (1996), in *Monte Carlo and Molecular Dynamics of Condensed Matter Systems*, eds. K. Binder and G. Ciccotti (Società Italiana di Fisica, Bologna).

Young, A. P. (ed.) (1998), *Spin Glasses and Random Fields* (World Scientific, Singapore).

Zorn, R., Herrmann, H. J., and Rebbi, C. (1981), *Comput. Phys. Commun.* **23**, 337.